# Uncovering the Computational Ingredients of Human-Like Representations in LLMs

Zach Studdiford\*
University of Wisconsin–Madison

**Timothy Rogers**University of Wisconsin–Madison

Kushin Mukherjee<sup>1</sup> Stanford University

Siddharth Suresh\*1

University of Wisconsin-Madison

### **ABSTRACT**

The ability to translate diverse patterns of inputs into structured patterns of behavior has been thought to rest on both humans' and machines' ability to learn robust representations of relevant concepts. The rapid advancement of transformer-based large language models (LLMs) has led to a diversity of computational ingredients — architectures, fine tuning methods, and training datasets among others — but it remains unclear which of these ingredients are most crucial for building models that develop human-like representations. Further, most current LLM benchmarks are not suited to measuring representational alignment between humans and models, making existing benchmark scores unreliable for assessing if current LLMs are making progress towards becoming useful cognitive models. Here, we address these limitations by first evaluating a set of over 77 models that widely vary in their computational ingredients on a triplet similarity task, a method well established in the cognitive sciences for measuring human conceptual representations, using concepts from the THINGS database. Comparing human and model representations, we find that models that undergo instruction-finetuning and which have larger dimensionality of attention heads are among the most human aligned. We also find that factors such as choice of activation function, multimodal pretraining, and parameter size have limited bearing on alignment. Correlations between alignment scores and scores on existing benchmarks reveal that while some benchmarks (e.g., BigBenchHard) are better suited than others (e.g., MUSR) for capturing representational alignment, no existing benchmark is capable of fully accounting for the variance of alignment scores, demonstrating their insufficiency in capturing human-AI alignment. Taken together, our findings help highlight the computational ingredients most essential for advancing LLMs towards models of human conceptual representation and address a key benchmarking gap in LLM evaluation.

### 1 Introduction

The success of deep neural network models on diverse domains ranging from perception (Yamins et al., 2014; Yamins & DiCarlo, 2016), to robotic manipulation (Finn et al., 2016), to language understanding (Tuckute et al., 2024) has partly been attributed to their ability to learn powerful representations that can effectively aid in translating inputs into appropriate outputs. The continued development of a specific class of these systems — transformer-based large language models (LLMs) — and their capabilities on naturalistic human tasks might imply that these models, through training on large enough corpora of text (and often image) data and with the correct architectural ingredients, come to possess representations that are largely isomorphic to humans' mental representations. This implication is critical for many domains of cognitive science that have long sought to characterize the nature of human conceptual representations and the operations

<sup>\*</sup>Correspondence to: Zach Studdiford (studdiford@wisc.edu) and Siddharth Suresh (siddharth.suresh@wisc.edu).

<sup>&</sup>lt;sup>1</sup>Equal contribution.

performed on them that lead to naturalistic behavior. Indeed, there is a rich tradition of using deep neural networks as *computational cognitive models*: using their learned representations as proxies for human representations, and often mapping the evolution of learned representations to development of human conceptual representations (Jackson et al., 2022; Warstadt et al., 2025). While a patchwork of evidence in various domains has shown concordances in representations between language models and people's behaviors and patterns in their neural activity, it remains unclear what properties of current LLMs are most predictive of strong human-model alignment. That is, given the engineering-centric drive behind current LLM development, it is difficult to isolate what *computational ingredients* (model architecture, model size, instruction-tuning, activation functions, etc.) are important for giving rise to human-aligned conceptual representations in models for a large variety of concepts.

Identifying the computational ingredients underlying human-model alignment is critical for several reasons. While frontier models have achieved remarkable performance on diverse benchmarks spanning scientific reasoning (Rein et al., 2024; Suzgun et al., 2022), software engineering (Chen et al., 2021; Jimenez et al., 2023), and chart and humor understanding (Masry et al., 2022; Methani et al., 2020; Mukherjee et al., 2025; Zhou et al., 2025; Hessel et al., 2022) (domains thought to require 'human-like' thinking), we lack a unified theory explaining *why* model performance on one task might transfer to another and reasons for inconsistencies in benchmark rankings for the same model. Recent work has shown that optimizing for benchmark accuracy alone is insufficient for building models that fail in human-like ways and that are generally aligned with humans (Fel et al., 2022; Ying et al., 2025). We argue that prioritizing representational alignment (Sucholutsky et al., 2023; Sucholutsky & Griffiths, 2023b; Muttenthaler et al., 2024) offers a promising path forward. Measuring the similarity between model and human internal representations can provide a more unified account of model capabilities, guide the development of more robustly aligned systems (Collins et al., 2024; Muttenthaler et al., 2024; Peterson et al., 2018), and accelerate cognitive science by yielding more faithful computational models of the human mind.

### 2 Related work

Quantifying Human and Model Representations using Large-Scale Concept Datasets Mapping the geometry human conceptual knowledge has long been a central goal of cognitive science (Rogers & McClelland, 2004; Shepard, 1980; Tversky, 1977; Rumelhart et al., 1986). Early attempts to do so relied on explicit feature ratings and pairwise similarity judgments, which scaled poorly limiting their utility in capturing the structure of the vast inventory of human concepts (Rosch, 1975; Nosofsky, 1984; Shepard, 1980). While structured probabilistic models have been useful in explaining aspects of concept learning, they too have been limited often being restricted to specific relational structures, limiting their scope and generalizability (Zhao et al., 2024; Wong et al., 2022; Kemp & Tenenbaum, 2008). Recent years have seen a resurgence of similarity-based measures of characterizing human conceptual knowledge, driven by scalable algorithms that convert human judgments into expressive high-dimensional semantic embeddings (King et al., 2019; Mukherjee & Rogers, 2025; Hebart et al., 2019; Suresh et al., 2023b; Peterson et al., 2018; Kriegeskorte & Mur, 2012; Cichy et al., 2019; Hebart et al., 2023; Muttenthaler et al., 2022b; Jamieson et al., 2015; Sievert et al., 2023) capable of expressing latent dimensions organizing human semantic knowledge. Specifically, triadic similarity judgment tasks — where participants select the most similar item from a triplet—are a particularly powerful paradigm (Tamuz et al., 2011; Wah et al., 2014; Kleindessner & von Luxburg, 2014). Embeddings derived from this measure have shown to be good predictors of both neural and behavioral patterns in humans across a variety of semantic tasks (Mukherjee & Rogers, 2025; Mukherjee et al.; Hebart et al., 2023; Colon & Rogers, 2023; Suresh et al., 2023b; Marjieh et al., 2022; Mukherjee et al., 2022; Mur et al., 2013; Suresh et al., 2024).

A complementary advancement in recent years that has galvanized research in representational alignment is the development of concept datasets that aim to capture the diversity of object concepts humans reason about (Mehrer et al., 2021; Hebart et al., 2019; Giallanza et al., 2024; Suresh et al., 2025). Datasets like THINGS (Hebart et al., 2019) and ECOSET (Mehrer et al., 2021) consist of concept sets and associated images along with rich psychological and neural metadata (Hebart et al., 2023) that allow for rich comparisons between human and model representations along multiple levels of analysis — behavioral, neural, and computational.

Representational Alignment: Measurement and Downstream Task Performance The nascent field of representational alignment has developed formal tools for comparing internal representations across biological and artificial systems (Kriegeskorte et al., 2008; Sucholutsky et al., 2023; Barbosa et al., 2025; Oswal et al., 2016). Core measurement techniques include Representational Similarity Analysis (RSA) using correlation between similarity matrices derived from behavioral, neural, or neural network activation data (Kriegeskorte et al., 2008; Nili et al., 2014), Procrustes analysis for finding optimal linear alignments (Schönemann, 1966), and Centered Kernel Alignment (CKA) for comparing representations invariant to linear transformations (Kornblith et al., 2019; Williams et al., 2021). Recent work has further developed more sensitive metrics including shape-based metrics (Williams et al., 2021), topological measures (Barannikov et al., 2021), informationtheoretic approaches (Bansal et al., 2021), and regularized regression-based methods Oswal et al. (2016) each of which iteratively address issues relating to model regularization, generalization, and error-bounds. Growing evidence demonstrates that representational alignment with humans correlates with practical benefits for model performance. Models with higher human alignment show improved few-shot learning (Sucholutsky & Griffiths, 2023a; Huh et al., 2024), better outof-distribution generalization (Moschella et al., 2023; Norelli et al., 2023), enhanced adversarial robustness (Engstrom et al., 2019), and more human-like error patterns (Geirhos et al., 2021; Fel et al., 2022). These findings suggest that human-aligned representations capture meaningful invariances that support robust intelligence.

Computational Ingredients Driving Alignment Understanding which design choices yield human-aligned representations in foundation models can help uncover general principles undergirding human intelligence. For instance, in vision, early work showed that optimizing models for categorization (Yamins et al., 2014) and later for contrastive objectives (Konkle & Alvarez, 2022; Zhuang et al., 2021) produced representations closely aligned with activity in the human visual cortex, offering insight into the kinds of objective functions the brain may solve to construct visual representations. Extending this line of inquiry, Muttenthaler et al. (2022a) evaluated over 75 models spanning architectures, objectives, and datasets, and found that training data and objectives strongly predicted human-model alignment, whereas architecture and scale had minimal impact. This finding challenges scaling law accounts (Kaplan et al., 2020; Cherti et al., 2023) that predict generally larger models should always perform better (at most tasks). Other key findings regarding the importance of different computational ingredients include the finding that self-supervised contrastive methods align more closely with human vision than non-contrastive approaches (Chen et al., 2020; Zbontar et al., 2021; Caron et al., 2020); multimodal image-text contrastive training improves alignment over vision-only training (Radford et al., 2021; Jia et al., 2021; Pham et al., 2022); training on diverse, naturalistic datasets such as JFT-3B improves alignment beyond ImageNet (Zhai et al., 2022; Dehghani et al., 2023); enforcing shape bias on models enhances alignment while texture bias impairs it (Geirhos et al., 2019; Hermann et al., 2020); and intermediate layers often show stronger perceptual alignment than final layers (Berardino et al., 2017; Kumar et al., 2022). Similar approaches, dissecting the predictive power of different model building choices, have not been brought to bear in investigations into conceptual structure in LLMs- leaving unclear what the relative importance of different computational ingredients are when building foundation models of human semantic knowledge.

Language Models and Conceptual Alignment Recent work has begun extending analyses of representational alignment to language models (Suresh et al., 2023b; Marjieh et al., 2022). Early studies showed that contextualized embeddings from models like BERT and GPT-2 could predict human similarity judgments (Bommasani et al., 2020; Grand et al., 2022). More recent work demonstrates that LLMs can achieve remarkably high alignment with human conceptual structure (Marjieh et al., 2024a;b; Mukherjee et al., 2024; Suresh et al., 2025; 2023a; Mukherjee et al., 2023b), with instruction-tuned models showing particular advantages (Tong et al., 2024; Gurnee & Tegmark, 2024). Several studies have used triplet tasks specifically to probe LLM representations (Nam et al., 2024; Studdiford et al., 2025; Rathi et al., 2024; Suresh et al., 2023b), finding that larger models and those trained on more diverse data show better alignment. However, systematic analyses disentangling the effects of scale, architecture, training data, and objectives remain limited. Work on multimodal models suggests that vision-language training improves conceptual alignment beyond either modality alone (Yuksekgonul et al., 2023; Thrush et al., 2022; Qin et al., 2025), though the mechanisms remain unclear.

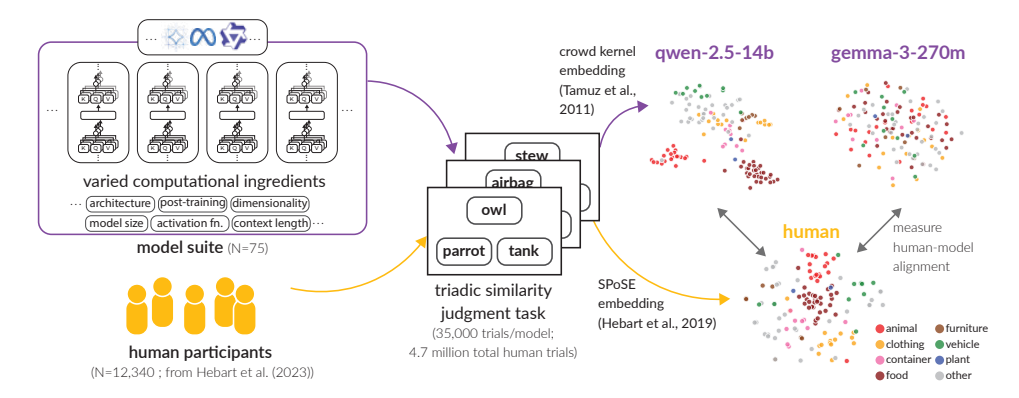


Figure 1: *Method for estimating human-model alignment.* We collected 35k triplet similarity judgments from each of the 77 models in our suite. We computed semantic embeddings based on these judgments and compared the representational geometry of model embeddings to human embeddings derived from Hebart et al. (2023).

Summary of key contributions. We leverage the open-weight model ecosystem to construct a suite of 75+ models spanning diverse computational ingredients. Using concepts and semantic embeddings from THINGS dataset (Hebart et al., 2019) in conjunction with a triadic similarity judgment paradigm (Jamieson et al., 2015; Hebart et al., 2023; Sievert et al., 2023), we obtain both human and model-specific conceptual embeddings using analogous methods to ensure model-fair comparisons (Firestone, 2020). We then compare these embeddings to human data and apply statistical models to identify the ingredients most predictive of human-model alignment. Lastly, we relate alignment to performance on standard LLM benchmarks, highlighting points of convergence and divergence between representational alignment and task capabilities.

### 3 METHODS

Concept Dataset To investigate how various LLM characteristics influence human alignment, we carefully curated a set of test concepts that would provide robust and interpretable results. Starting from the full set of 1,854 THINGS object concepts (Hebart et al., 2019; 2023), we subsampled 128 concrete, real-world object concepts (e.g., "lion", "banjo", "car") that spanned four main cognitive axes of variation: familiarity, artificiality, animacy, and size based on prior work (Mukherjee et al., 2023a). This sampling strategy ensured that we had adequate semantic diversity in our concept dataset (representative of the full THINGS database) while also ensuring that we could generate semantic embeddings for a large suite of models at scale in a tractable manner. The complete list of object concepts, along with detailed descriptions of our concept selection criteria and validation procedures, can be found in Appendix A.3.

**Model Suite** We evaluate a range of open-source models varying across several key computational ingredients: model architecture, primary activation functions used, pre-training modality, whether models were instruction fine-tuned or not, scale (both in terms of model parameters and training tokens), context length, dimensionality of attention heads/MLPs/residual streams. While in principle it is possible to offer even more granular analyses of computational ingredients, these factors constitute major architectural and training decisions when building foundation models, which we believe provide adequate resolution to investigate the drivers of human-model alignment.

We evaluated a set of 77 open-weight transformer models including models from popular families (Llama, Qwen, Gemma, etc.). The full set of models can be seen in Table 4. Notably, we included models that varied in size from 100M parameters to 42B parameters, ranged in the degree of post-training (from base to instruction fine-tuned), and architecture-style (decoder-only, encoder-decoder, and state space models (SSMs) (Voelker & Eliasmith, 2018)).

**Triadic similarity judgment task** The triadic similarity judgment task can be framed in two equivalent ways: (1) **anchored similarity judgments** where participants are presented with a triplet of items (images or words depicting different concepts) and select which of two option items is most similar to an anchored reference item, or **odd-one-out judgments** where they identify which

of the three presented item is the odd-one-out. Both framings have been successfully employed to study conceptual representations in humans and models (Hebart et al., 2019; 2023; Mukherjee et al., 2023c; Colon & Rogers, 2023; Suresh et al., 2023b; Studdiford et al., 2025; Mukherjee et al.; Muttenthaler et al., 2022b). In this work, we leverage existing human similarity ratings data (Hebart et al., 2023) and corresponding embeddings, which were collected using the oddone-out paradigm and embedded using the sparse positive similarity embedding (SPoSE) method, respectively. For model evaluations, we adopted the anchored similarity judgment paradigmn for computational efficiency, deriving embeddings using ordinal embedding techniques (Jamieson et al., 2015; Tamuz et al., 2011) following recent work (Suresh et al., 2023b; Mukherjee et al.; Colon & Rogers, 2023). Crucially, the ordinal embedding approach provides theoretical bounds on sample complexity (Jamieson et al., 2015), allowing us to determine the number of triplet comparisons needed for faithful representations a priori (see Section 3 for details). While these approaches differ in framing and embedding computation, they yield comparable representational structures. This methodological choice allows us to maximize the use of existing high-quality, validated human data while efficiently collecting model responses with known sampling requirements in a scalable manner, ensuring robust human-model comparisons across a large suite of models.

**Human Semantic Embeddings** Human semantic embeddings were obtained by Hebart et al. (2023) from the behavioral judgments of N=12,340 online participants in a triplet odd-one-out task. On each trial, participants were shown three items from the THINGS database and were prompted to select the most dissimilar object("Which is the odd one out?"). In total, 4.7 million behavioral triplet judgments were obtained for the full set of 1,854 concepts. To estimate an embedding space from the set of individual triplet judgments, Hebart et al. (2023) used the SPoSE algorithm (Hebart et al., 2023), which learns low-dimensional vectors for each object such that (1) pairs of objects judged as similar are placed closer in the embedding space, and (2) dimensions are constrained to be sparse in order to yield human-interpretable properties. The resulting space captured meaningful representational structure from the individual judgments of participants, revealing core dimensions along which human semantic representations are organized.

Model Semantic Embeddings While much work assessing representational similarity between models and humans focus on extracting activation vectors from models and computing their similarity to human behavior-based representations (using methods like RSA (Kriegeskorte et al., 2008)), we instead estimated model semantic embeddings from model similarity judgments using a triadic comparison task akin to those often used to estimate human embeddings. We did so for two principled reasons. Firstly, while computations in transformer layers and attention heads have been linked to human language processing (Tuckute et al., 2024), there is no general framework for assessing which parts (layers, heads) of models (across different model families) are likely to carry signature of human semantic knowledge, making it difficult to assess what constitutes a fair comparison between model activations and human representations. Second, due to the ability of modern LLMs to respond to structured tasks when prompted in natural language and given the relative simplicity of the triadic judgment task (often single token responses suffice), we felt that administering the same test to both models and humans constitutes a species-fair (Firestone, 2020) comparison approach. Further, this allows for a unified embedding method to be applied to both systems ensuring that any discrepancies in alignment are not attributable to vastly different embedding methods.

For each model in our suite, we collected 35,000 triadic judgment responses. Using the human semantic embeddings, we estimated that a rank 30 space explains over 95% of the variance in embeddings (see A.7). Based on known bounds (Sievert et al., 2023), we require  $(n \cdot d \cdot log_2(n)^1) \approx 26,900$  judgments on random sets of triplets to estimate a robust embedding. We collected 35,000 to account for noise in the judgments. Each triplet trial was randomly sampled from the  $\binom{128}{3}$  possible triplet trials. We evaluated each model using its default huggingface sampling settings using a common system-level prompt — "You are a helpful assistant who gives responses to questions". We used the following prompt for each trial for each model — QUESTION: Which item is most similar to item\_x: item\_y or item\_z? Respond only with the item name. If we were evaluating a base

 $<sup>^{1}</sup>n$  is the number of items and d is the expected dimensionality of the space

model (not instruction-tuned), we appended Answer: after the initial prompt. Specific instruction template formats were applied where appropriate. Each prompt was evaluated independently.

Using these similarity judgments, we fit an ordinal embedding algorithm (Tamuz et al., 2011; Sievert et al., 2023) that organized the semantic embedding space such that items that were judged to be similar more often were pulled closer together in this space. We fit 30D embeddings based on the dimensionality of human semantic embeddings. We also held out 20% of the data during the embedding fitting process and evaluated the quality of the embeddings by monitoring the crowd-kernel loss (Tamuz et al., 2011) to ensure the embeddings were of high quality.

### 4 RESULTS AND DISCUSSION

We first report on how predictive different computational ingredients were of human-model alignment, initially considering each ingredient separately via individual correlations or t-tests (Kim, 2015), then assessing relative contributions of each via mixed linear models (Lindstrom & Bates, 1988). Finally, we evaluate the relationship between human-model alignment and model performance on other key LLM benchmarks (Han et al., 2024; Rein et al., 2023; Srivastava et al., 2023; Zhou et al., 2024; Hendrycks et al., 2020). Our primary alignment measure was the variance in human semantic embeddings explained by model embeddings ( $R^2$ ) after Procrustes alignment (Gower, 1975). Procrustes transforms find the optimal linear transformation (rotation, scaling, translation) between two vector spaces of equal dimensionality to minimize squared distances between corresponding points. Using human embedding variance (human SS) as the baseline, we compute  $R^2 = 1 - \frac{\text{residual SSE}}{\text{human SSE}}$ . Other alignment measures such as CKA (Kornblith et al., 2019) and RSA(Kriegeskorte et al., 2008) were highly correlated with Procrustes  $R^2$  (Appendix A.7).

#### 4.1 Contributions of Model Computational Ingredients to Alignment

Instruction tuning leads to greater alignment. Models with instruction fine-tuning were significantly better aligned than those without (t=5.11, p<0.001; see Figure 2A). Qualitatively, instruction fine-tuning clusters the representations of semantic categories, such that within-category items become more proximal in representation space and between-category items become more distal (see Appendix 7). Thus, the same post-training techniques that enable models to be more adept at following prompt instructions also bring their representations closer into alignment with humans'.

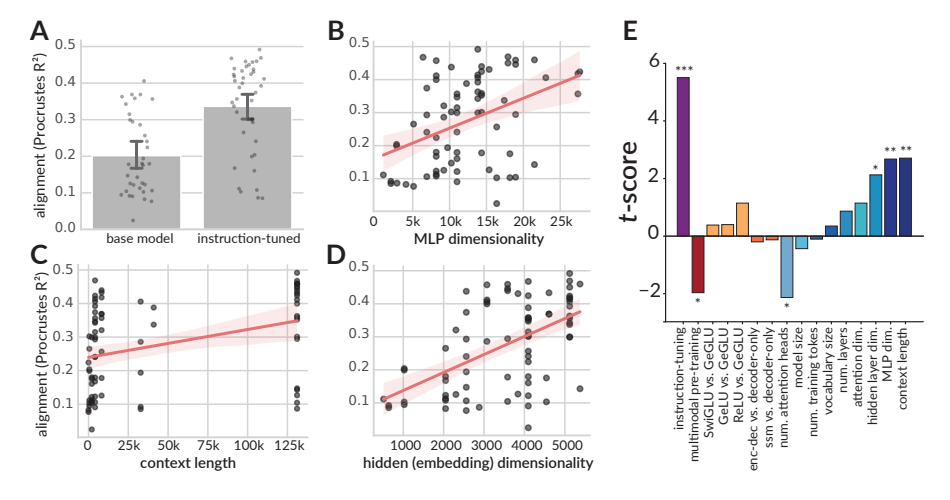


Figure 2: Computational ingredients predictive of human model alignment. A., B., C., and D. show the relationship between instruction-tuning, MLP dimensionality, context length, and embedding dimensionality on Procrustes  $\mathbb{R}^2$ . These were the four ingredients most predictive in the mixed-effects regression model. E. t-scores for each predictor, which highlight the relative contribution of each ingredient towards alignment when considered in a single statistical model.

**Model architecture dimensionality corresponds to greater alignment.** We found a strong positive relationship between the dimensionality of individual model architecture components — MLPs and attention heads — and the degree of model-human alignment. Specifically, the number of per-layer attention heads (r=0.52, p<0.001), attention matrix dimensionality (r=0.30, p=0.026), embeddings dimensionality (r=0.54, p<0.001), and MLP dimensionality (r=0.40, p<0.001) each correlated positively with human representational alignment. Figure 2B and D show the individual correlations between MLP and embedding dimensionality and model-human Procrustes  $R^2$  (the attention dimensionality was not significant in multiple regression models reported in subsequent sections). Thus the greater expressivity granted by larger latent activation spaces and more attention heads predicts greater human alignment.

**Multi-modal pretraining has no effect on alignment.** While much of human concept learning is inherently multimodal (Rogers & McClelland, 2004; Patterson et al., 2007), there is limited work showing whether vision-language pretraining (the most prominent class of multimodal training) leads to more aligned semantic representations (cf. (Qin et al., 2025)). In our model suite, however, multimodal (image) pre-training had no independent effect on human-model alignment relative to text-only models (t=0.34, p>0.05; Appendix Figure A.8).

Larger model sizes showed greater human alignment. For visual representations, Muttenthaler et al. (2022a) found that larger models need not yield more human-like representations. Neural scaling laws (Kaplan et al., 2020), however, might predict that larger and deeper models should be more performant, and perhaps more aligned. In accordance with this prediction, human-model alignment scaled approximately linearly with both model parameter count and the number of model layers ( $r_{param}=0.45, r_{layers}=0.41, p<0.001$ ; Appendix Figure A.8). Thus, larger scale predicts greater human-model alignment.

Alignment increased with amount of training data. Models exposed to more tokens in pretraining generally exhibited more human-like representations ( $r=0.33,\,p<0.01$ ; Appendix Figure A.8). Although model training data also likely varied in quality and composition—thus limiting strong conclusions about which properties matter most—our results indicate that the *amount* of training data can predict alignment.

Alignment scales with context length. The triadic similarity task does not require a long context length, but we nevertheless found that models with a greater maximum context-length also demonstrated greater human alignment (r=0.35, p<0.01; Figure 2). This finding could be linked to post-training regimes that unlock long-context reasoning, which consequently lead models to perform well on short-context tasks as well.

Choice of activation function does not affect alignment. Activation functions have seen iterative development over the years with recent variants (e.g., SwiGLU (Shazeer, 2020)) being particularly well-suited to managing gradient flows during training and finetuning experiments leading to faster and more stable training regimes. But do choices in activation functions ground out in alignment? We found no advantage for any particular function in increasing human alignment (F(3, 64) = 1.36, p = .26; Appendix Figure A.8).

Larger vocabulary size does not increase alignment. One might expect that larger model vocabularies unlock greater expressivity for models, leading them to be more human-aligned. Against this prediction, we found no relationship between model vocabulary size and human-alignment (r = 0.10, p > 0.05; Appendix Figure A.8).

Which computational ingredients have the greatest relative contribution towards human-model alignment? Thus far, we have investigated how different computational ingredients impact human-model alignment in isolation. In reality, many of these ingredients vary across models at the same time, leaving open the questions of (1) which ingredients are most important *relative to others* and (2) which ingredients account for unique variance after others are considered.

To answer these questions, we fit a mixed-effects multiple regression model (Lindstrom & Bates, 1990) predicting Procrustes  $\mathbb{R}^2$  from all computational ingredients. Mixed-effects models combine the interpretability of OLS with random effects to capture item-level variance (Barr et al., 2013). We included random intercepts for model family (e.g., Llama, Qwen) to capture variance related to these families not grounded out in our set of ingredients, and fixed effects for all ingredients. The fitted model explained substantial variance in alignment ( $\mathbb{R}^2 = 0.78$ ; Fig. 2E). Instruction fine-

tuning emerged as the strongest predictor ( $\beta=0.13$ , SE=0.024, p<0.001). Dimensionality measures — MLP ( $\beta=0.049$ , SE=0.018, p<0.01), embedding/hidden layers ( $\beta=0.048$ , SE=0.022, p<0.05) — and context length ( $\beta=0.042$ , SE=0.015, p<0.01) also accounted for significant unique variance. In contrast to the independent analyses, attention dimensionality was not significant, and more attention heads predicted worse alignment after accounting for other factors ( $\beta=-0.045$ , p<0.05). Likewise, multimodal pretraining, which showed no independent effect on alignment, predicted reliably lower alignment after accounting for other factors ( $\beta=-0.102$ , SE=0.052, p<0.05). Thus, current multimodal training regimes may actually limit rather than improving human-model alignment. No other ingredient explained significant unique variance when others were included in the mode (see effect sizes in Figure 2E).

A case study on the effects of post-training paradigms on alignment. Modern LLM systems undergo various stages of post-training including *supervised fine-tuning* (SFT) (Ouyang et al., 2022), *direct preference optimization* DPO (Rafailov et al., 2023), *reinforcement learning from human feedback* (RLHF) (Ouyang et al., 2022), and *instruction tuning* (IT) (Wei et al., 2021). It remains unclear what impact these post-training steps have on human-model alignment. Progress on this front has been limited due to a lack of open-weight models that have been checkpointed at the various possible stages. OLMO (Groeneveld et al., 2024) is a notable exception since it is available at four stages of post-training, including the base model (no post-training), SFT, DPO, and IT and is available at two model sizes (7B and 13B). Instella (Liu et al., 2025) and Llama-3.1 (Meta AI, 2024) also have similar checkpointed model variants available with Instella having an additional stage of pretraining checkpointed.

Using these models, we asked whether successive stages of post-training led to models' representations becoming more aligned with humans'. Figure 3 shows how alignment changes as a function of post-training. Generally, we found that the SFT and DPO stages led to improvements in alignment whereas the effect of RLVR was more muted.

### 4.2 RELATIONSHIP BETWEEN ALIGNMENT AND ESTABLISHED BENCHMARKS

Prior work emphasizes that performance on a given model evaluation should "translate to similar improvements on any other valid and reasonable evaluation data" (Bowman & Dahl, 2021). But these arguments were developed in the context of specific NLP tasks, leaving it unclear whether this notion extends to representational alignment. To understand the relationship between alignment and performance on standard LLM benchmarks we estimated the correlation between alignment, measured using three metrics (Procrustes  $R^2$ , CKA, and RSA correlation), and model scores on five key benchmarks – MMLU, IFEval, BigBenchHard (BBH), GPQA, and MUSR. Figure 4A shows the relationship between alignment (Procrustes  $R^2$ ) and scores on BBH, the benchmark most strongly correlated with alignment.

While models that performed well on BBH generally had stronger alignment, we found some notable divergences especially for base models that scored lower on alignment than one might expect based on their BBH score. Figure 4B shows the correlations between alignment and all the established benchmarks. While all three alignment metrics were in agreement, we found that the overall correlations varied ( $r_{min}=0.36, p<0.05; r_{max}=0.74, p<0.001$ ). We focus on Procrustes  $R^2$  moving forward.

Performance on benchmarks that probe probe domain-general knowledge (BBH; r=0.74, p<0.001; MMLU; r=0.71, p<0.001) and instruction-following ability (IFEval; r=0.68, p<0.001) were

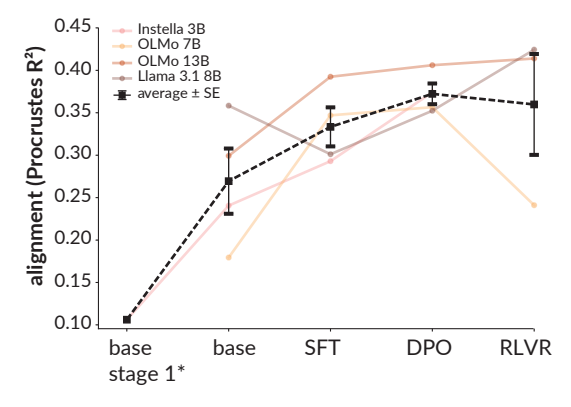


Figure 3: **Effects of post-training on alignment**. The black points show mean alignment (across models) at each post-training stage.\*Instella only.

more correlated with alignment than benchmarks testing more specific domain knowledge and reasoning ability (Math; r = 0.61, p < 0.001, MUSR; r = 0.36, p < 0.05).

This finding is sensible given that alignment with human semantic judgments requires representing semantic knowledge broadly in human-like ways (captured by BBH and MMLU) and deploying that knowledge in context-sensitive ways according to instructions (captured by IFEval). We also found that the correlation between BBH and IFEval was significantly weaker than the correlation between these evaluations and our measure of representational alignment( $r_{BBH,IFEval} = 0.44, p < 0.01$ ), suggesting our alignment measure captures separate competencies unique to each benchmark.

### 5 Conclusion

The rapid advancement of language models (both in scale and diversity) and the varied, often unpredictable, performance of models on standard benchmarks has left open the question "what does it take to make human-like models"? A gold standard for 'human-like' would be to have models that not only perform tasks in human-like ways but also have internal representations and computations that are similar to that of humans. Here we attempt to identify the computational ingredients most predictive of human-model representational alignment.

We first leveraged a large-scale dataset of human triadic similarity judgments and associated semantic embeddings from the THINGS dataset and set them as the target for measuring alignment. Next, we carefully constructed a suite of 77 open-weight language models that varied in several key computational ingredients including model scale, training dataset size, dimensionality of model embeddings, and post-training regimes, among others. We estimated semantic embeddings for each model using a triadic similarity judgment task analogous to the human task and measured representational alignment between model and human embeddings as function of different model characteristics. We arrived at several key insights.

First, we found two convergent pieces of evidence that modern post-training techniques are central to human-model alignment: (1) instruction-finetuning was the strongest predictor of alignment even after controlling for variance explained by other ingredients (Figure 2 and (2) alignment tended to increase across different stages of post-training (Figure The importance of context length in predicting alignment further suggests that the methods that enable long contextreasoning also bring model representations into closer alignment with humans. Second, we observed that architectural dimensionality (embedding layers, MLP) were relatively more important than overall model size and training corpus size in predicting alignment, especially in the mixed-effects model suggesting that representational capacity is key to developing models that align with human representations. Third, we found that while some existing benchmarks were correlated with our measure of alignment (e.g., MMLU, BBH), no single benchmark captured all the variance in representational alignment. Notably, benchmarks emphasizing broad semantic knowledge and its flexible deployment showed the strongest correlations, consistent with the-

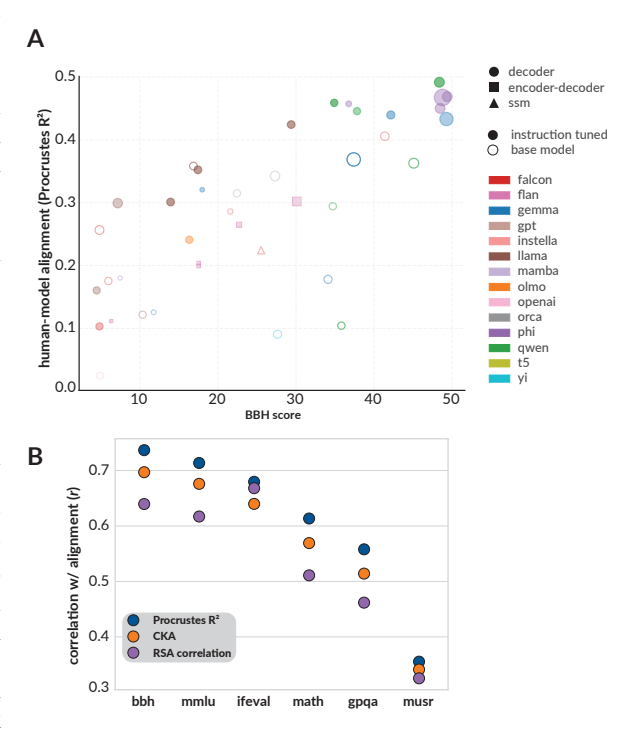


Figure 4: Relationship between alignment and other LLM benchmarks. A. BigBenchHard scores for each model in our suite vs. their Procrustes  $\mathbb{R}^2$  value w.r.t. human embeddings. B. Correlation between alignment and the six LLM benchmarks evaluated.

ories of how humans represent semantic knowledge (Rogers & McClelland, 2004; Saxe et al., 2019).

**Limitations** To our knowledge, this is the first attempt to isolate the computational ingredients predictive of human–LLM conceptual alignment in language models, however several limitations remain that future work could address. <u>First</u>, while we evaluated many core computational ingredients, we could not assess the role of training dataset composition (e.g., text–code balance, language coverage) due to limited documentation for many models. Future work should look beyond token counts to clarify which dataset properties enable semantic alignment. <u>Second</u>, some classes of models were sparsely represented in our suite including SSMs, multimodal models, and mixture-of-expert models limiting the reliability of insights we can derive regarding ingredients that support them. <u>Third</u>, while similarity judgements are a well validated method and scale well to large concept sets, there may be other ways of probing semantic knowledge such as by observing how models deploy this knowledge in open-ended reasoning tasks (Wong et al., 2025; Mahowald et al., 2024). Future work can seek to study such tasks that tackle the *deployment* of semantic knowledge.

### REFERENCES

- 01.AI Team. Yi: Open foundation models. arXiv:2403.04652, March 2024.
- Yamini Bansal, Preetum Nakkiran, and Boaz Ravikumar. Revisiting model stitching to compare neural representations. *Advances in neural information processing systems*, 34:225–236, 2021.
- Serguei Barannikov, Ilya Trofimov, Nikita Balabin, and Evgeny Burnaev. Representation topology divergence: A method for comparing neural network representations. *arXiv preprint arXiv:2201.00058*, 2021.
- Joao Barbosa, Amin Nejatbakhsh, Lyndon Duong, Sarah E Harvey, Scott L Brincat, Markus Siegel, Earl K Miller, and Alex H Williams. Quantifying differences in neural population activity with shape metrics. *bioRxiv*, pp. 2025–01, 2025.
- Dale J Barr, Roger Levy, Christoph Scheepers, and Harry J Tily. Random effects structure for confirmatory hypothesis testing: Keep it maximal. *Journal of memory and language*, 68(3):255–278, 2013.
- Alexander Berardino, Valero Laparra, Johannes Ballé, and Eero Simoncelli. Eigen-distortions of hierarchical representations. *Advances in neural information processing systems*, 30, 2017.
- S. Black, S. Biderman, et al. Gpt-neox-20b: An open-source autoregressive language model. In *Proceedings of Machine Learning and Systems*, April 2022. [Online]. Available: https://aclanthology.org/2022.mlsys-1.72.
- Rishi Bommasani, Kelly Davis, and Claire Cardie. Interpreting pretrained contextualized representations via reductions to static embeddings. *Proceedings of the 58th Annual Meeting of the Association for Computational Linguistics*, pp. 4758–4781, 2020.
- Samuel R. Bowman and George Dahl. What will it take to fix benchmarking in natural language understanding? In Kristina Toutanova, Anna Rumshisky, Luke Zettlemoyer, Dilek Hakkani-Tur, Iz Beltagy, Steven Bethard, Ryan Cotterell, Tanmoy Chakraborty, and Yichao Zhou (eds.), Proceedings of the 2021 Conference of the North American Chapter of the Association for Computational Linguistics: Human Language Technologies, pp. 4843–4855, Online, June 2021. Association for Computational Linguistics. doi: 10.18653/v1/2021.naacl-main.385. URL https://aclanthology.org/2021.naacl-main.385/.
- Mathilde Caron, Ishan Misra, Julien Mairal, Priya Goyal, Piotr Bojanowski, and Armand Joulin. Unsupervised learning of visual features by contrasting cluster assignments. *Advances in neural information processing systems*, 33:9912–9924, 2020.
- Mark Chen, Jerry Tworek, Heewoo Jun, Qiming Yuan, Henrique Ponde De Oliveira Pinto, Jared Kaplan, Harri Edwards, Yuri Burda, Nicholas Joseph, Greg Brockman, et al. Evaluating large language models trained on code. *arXiv preprint arXiv:2107.03374*, 2021.

- Ting Chen, Simon Kornblith, Mohammad Norouzi, and Geoffrey Hinton. A simple framework for contrastive learning of visual representations. *International conference on machine learning*, pp. 1597–1607, 2020.
- Mehdi Cherti, Romain Beaumont, Ross Wightman, Mitchell Wortsman, Gabriel Ilharco, Cade Gordon, Christoph Schuhmann, Ludwig Schmidt, and Jenia Jitsev. Reproducible scaling laws for contrastive language-image learning. In *Proceedings of the IEEE/CVF conference on computer vision and pattern recognition*, pp. 2818–2829, 2023.
- H. W. Chung, L. Hou, et al. Scaling instruction-finetuned language models. arXiv:2210.11416, December 2022. [Online]. Available: https://arxiv.org/abs/2210.11416.
- Radoslaw M Cichy, Nikolaus Kriegeskorte, Kamila M Jozwik, Jasper JF van den Bosch, and Ian Charest. The spatiotemporal neural dynamics underlying perceived similarity for real-world objects. *NeuroImage*, 194:12–24, 2019.
- Katherine M Collins, Ilia Sucholutsky, Umang Bhatt, Kartik Chandra, Lionel Wong, Mina Lee, Cedegao E Zhang, Tan Zhi-Xuan, Mark Ho, Vikash Mansinghka, et al. Building machines that learn and think with people. *Nature human behaviour*, 8(10):1851–1863, 2024.
- Y Ivette Colon and Timothy T Rogers. Yours and ours: Individual and group differences in semantic organization from triplet judgements of faces. In *Proceedings of the annual meeting of the cognitive science society*, volume 45, 2023.
- T. Dao, A. Gu, M. Mazeika, et al. Mamba: Linear-time sequence modeling with selective state spaces. arXiv:2312.00752, December 2023. [Online]. Available: https://arxiv.org/abs/2312.00752.
- Mostafa Dehghani, Josip Djolonga, Basil Mustafa, Piotr Padlewski, Jonathan Heek, Justin Gilmer, et al. Scaling vision transformers to 22 billion parameters. *arXiv preprint arXiv:2302.05442*, 2023.
- EleutherAI. Gpt-j-6b: 6 billion parameter open source gpt model. EleutherAI Blog, June 2021. [Online]. Available: https://6b.eleuther.ai.
- Logan Engstrom, Andrew Ilyas, Shibani Santurkar, Dimitris Tsipras, Brandon Tran, and Aleksander Madry. Adversarial robustness as a prior for learned representations. *arXiv* preprint *arXiv*:1906.00945, 2019.
- Falcon-LLM Team. The falcon 3 family of open models. Published Dec 2024. [Online]. Available: https://huggingface.co/blog/falcon3, December 2024.
- Thomas Fel, Ivan Felipe, Drew Linsley, and Thomas Serre. Harmonizing the object recognition strategies of deep neural networks with humans. *Advances in Neural Information Processing Systems*, 35:9432–9446, 2022.
- Chelsea Finn, Ian Goodfellow, and Sergey Levine. Unsupervised learning for physical interaction through video prediction. *Advances in neural information processing systems*, 29, 2016.
- Chaz Firestone. Performance vs. competence in human–machine comparisons. *Proceedings of the National Academy of Sciences*, 117(43):26562–26571, 2020.
- Robert Geirhos, Patricia Rubisch, Claudio Michaelis, Matthias Bethge, Felix A Wichmann, and Wieland Brendel. Imagenet-trained cnns are biased towards texture; increasing shape bias improves accuracy and robustness. *International Conference on Learning Representations*, 2019.
- Robert Geirhos, Kantharaju Narayanappa, Benjamin Mitzkus, Tizian Thieringer, Matthias Bethge, Felix A Wichmann, and Wieland Brendel. Partial success in closing the gap between human and machine vision. *Advances in Neural Information Processing Systems*, 34:23885–23899, 2021.
- Tyler Giallanza, Declan Campbell, Jonathan D Cohen, and Timothy T Rogers. An integrated model of semantics and control. *Psychological Review*, 2024.
- John C Gower. Generalized procrustes analysis. *Psychometrika*, 40(1):33–51, 1975.

- Gabriel Grand, Idan Asher Blank, Francisco Pereira, and Evelina Fedorenko. Semantic projection recovers rich human knowledge of multiple object features from word embeddings. *Nature Human Behaviour*, 6(7):975–987, 2022.
- D. Groeneveld, I. Beltagy, et al. Olmo: Accelerating the science of language models. arXiv:2402.00838, June 2024.
- S. Gunasekar, Y. Zhang, J. Aneja, et al. Textbooks are all you need. arXiv:2306.11644, October 2023.
- Wes Gurnee and Max Tegmark. Language models represent space and time. arXiv preprint arXiv:2310.02207, 2024.
- Sishuo Han, Wenshan Cheng, Zhiruo Liu, Kaixin Shi, Jing Zhou, Xiang Ren, and Yizhou Wang. MUSR: A multi-step unsupervised scientific reasoning benchmark. *arXiv* preprint *arXiv*:2405.08726, 2024.
- Martin N Hebart, Adam H Dickter, Alexis Kidder, Wan Y Kwok, Anna Corriveau, Caitlin Van Wicklin, and Chris I Baker. Things: A database of 1,854 object concepts and more than 26,000 naturalistic object images. *PLoS ONE*, 14(10):e0223792, 2019. doi: 10.1371/journal. pone.0223792.
- Martin N Hebart, Oliver Contier, Lina Teichmann, Adam H Rockter, Charles Y Zheng, Alexis Kidder, Anna Corriveau, Maryam Vaziri-Pashkam, and Chris I Baker. Things-data, a multimodal collection of large-scale datasets for investigating object representations in human brain and behavior. *eLife*, 12:e82580, 2023. doi: 10.7554/eLife.82580.
- Dan Hendrycks, Collin Burns, Steven Basart, Andy Zou, Mantas Mazeika, Dawn Song, and Jacob Steinhardt. Measuring massive multitask language understanding. *arXiv preprint arXiv:2009.03300*, 2020.
- Katherine Hermann, Ting Chen, and Simon Kornblith. The origins and prevalence of texture bias in convolutional neural networks. *Advances in Neural Information Processing Systems*, 33:19000–19015, 2020.
- Jack Hessel, Ana Marasović, Jena D Hwang, Lillian Lee, Jeff Da, Rowan Zellers, Robert Mankoff, and Yejin Choi. Do androids laugh at electric sheep? humor" understanding" benchmarks from the new yorker caption contest. *arXiv* preprint arXiv:2209.06293, 2022.
- Minyoung Huh, Brian Cheung, Tongzhou Wang, and Phillip Isola. The platonic representation hypothesis. *arXiv preprint arXiv:2405.07987*, 2024.
- Rebecca L Jackson, Matthew A Lambon Ralph, and Timothy T Rogers. Late maturation of executive control promotes conceptual development. *bioRxiv*, pp. 2022–03, 2022.
- Lalit Jain, Kevin Jamieson, and Robert Nowak. Finite sample prediction and recovery bounds for ordinal embedding, 2016. URL https://arxiv.org/abs/1606.07081.
- Kevin G. Jamieson and Robert D. Nowak. Active ranking using pairwise comparisons, 2011. URL https://arxiv.org/abs/1109.3701.
- Kevin G Jamieson, Lalit Jain, Chris Fernandez, Nicholas J Glattard, and Rob Nowak. Next: A system for real-world development, evaluation, and application of active learning. *Advances in neural information processing systems*, 28, 2015.
- R. Kumar, J. Ji, et al. Gemma: Open models based on gemini technology. research and Google Developers Blog, August https://developers.googleblog.com/en/ [Online]. Available: gemma-explained-overview-gemma-model-family-architectures/.
- Chao Jia, Yinfei Yang, Ye Xia, Yi-Ting Chen, Zarana Parekh, Hieu Pham, Quoc Le, Yun-Hsuan Sung, Zhen Li, and Tom Duerig. Scaling up visual and vision-language representation learning with noisy text supervision. *International Conference on Machine Learning*, pp. 4904–4916, 2021.

- Carlos E Jimenez, John Yang, Alexander Wettig, Shunyu Yao, Kexin Pei, Ofir Press, and Karthik Narasimhan. Swe-bench: Can language models resolve real-world github issues? *arXiv preprint arXiv:2310.06770*, 2023.
- Jared Kaplan, Sam McCandlish, Tom Henighan, Tom B Brown, Benjamin Chess, Rewon Child, Scott Gray, Alec Radford, Jeffrey Wu, and Dario Amodei. Scaling laws for neural language models. arXiv preprint arXiv:2001.08361, 2020.
- Charles Kemp and Joshua B Tenenbaum. The discovery of structural form. *Proceedings of the National Academy of Sciences*, 105(31):10687–10692, 2008.
- Tae Kyun Kim. T test as a parametric statistic. *Korean journal of anesthesiology*, 68(6):540–546, 2015.
- Marcie L King, Iris IA Groen, Adam Steel, Dwight J Kravitz, and Chris I Baker. Similarity judgments and cortical visual responses reflect different properties of object and scene categories in naturalistic images. *NeuroImage*, 197:368–382, 2019.
- Matthäus Kleindessner and Ulrike von Luxburg. Uniqueness of ordinal embedding. *Conference on Learning Theory*, pp. 40–67, 2014.
- Talia Konkle and George A Alvarez. A self-supervised domain-general learning framework for human ventral stream representation. *Nature communications*, 13(1):491, 2022.
- Simon Kornblith, Mohammad Norouzi, Honglak Lee, and Geoffrey Hinton. Similarity of neural network representations revisited. In *International Conference on Machine Learning*, pp. 3519– 3529. PMLR, 2019.
- Nikolaus Kriegeskorte and Marieke Mur. Inverse mds: Inferring dissimilarity structure from multiple item arrangements. *Frontiers in Psychology*, 3:245, 2012.
- Nikolaus Kriegeskorte, Marieke Mur, and Peter Bandettini. Representational similarity analysis—connecting the branches of systems neuroscience. *Frontiers in Systems Neuroscience*, 2:4, 2008.
- Manoj Kumar, Neil Houlsby, Nal Kalchbrenner, and Ekin D Cubuk. Do better imagenet classifiers assess perceptual similarity better? *Transactions on Machine Learning Research*, 2022.
- Mary J Lindstrom and Douglas M Bates. Newton—raphson and em algorithms for linear mixed-effects models for repeated-measures data. *Journal of the American Statistical Association*, 83 (404):1014–1022, 1988.
- Mary J Lindstrom and Douglas M Bates. Nonlinear mixed effects models for repeated measures data. *Biometrics*, pp. 673–687, 1990.
- J. Liu, J. Wu, et al. Introducing instella: New state-of-the-art fully open 3b language models. AMD ROCm Blog, March 2025. [Online]. Available: https://rocm.blogs.amd.com/artificial-intelligence/introducing-instella-3B/.
- Kyle Mahowald, Anna A. Ivanova, Idan A. Blank, Nancy Kanwisher, Joshua B. Tenenbaum, and Evelina Fedorenko. Dissociating language and thought in large language models, 2024. URL https://arxiv.org/abs/2301.06627.
- Raja Marjieh, Ilia Sucholutsky, Theodore R Sumers, Nori Jacoby, and Thomas L Griffiths. Predicting human similarity judgments using large language models. *arXiv preprint arXiv:2202.04728*, 2022.
- Raja Marjieh, Ilia Sucholutsky, Theodore R Sumers, Harin Lee, Thomas L Griffiths, and Nori Jacoby. Do large language models predict human similarity judgments? Cognitive Science, 48(8):e13509, 2024a.
- Raja Marjieh, Ilia Sucholutsky, Pol van Rijn, Nori Jacoby, and Thomas L Griffiths. Predicting human similarity judgments using large language models. *arXiv preprint arXiv:2402.10910*, 2024b.

- Ahmed Masry, Xuan Long Do, Jia Qing Tan, Shafiq Joty, and Enamul Hoque. Chartqa: A benchmark for question answering about charts with visual and logical reasoning. In *Findings of the Association for Computational Linguistics: ACL 2022*, pp. 2263–2279, 2022.
- Johannes Mehrer, Courtney J Spoerer, Emer C Jones, Nikolaus Kriegeskorte, and Tim C Kietzmann. An ecologically motivated image dataset for deep learning yields better models of human vision. *Proceedings of the National Academy of Sciences*, 118(8):e2011417118, 2021.
- Meta AI. Llama 3.1 8b instruct (2024 release). Internal technical report, Meta, 2024.
- Nitesh Methani, Pritha Ganguly, Mitesh M Khapra, and Pratyush Kumar. Plotqa: Reasoning over scientific plots. In *Proceedings of the ieee/cvf winter conference on applications of computer vision*, pp. 1527–1536, 2020.
- Luca Moschella, Valentino Maiorca, Marco Fumero, Antonio Norelli, Francesco Locatello, and Emanuele Rodolà. Relative representations enable zero-shot latent space communication. *arXiv* preprint arXiv:2209.15430, 2023.
- Kushin Mukherjee and Timothy T Rogers. Using drawings and deep neural networks to characterize the building blocks of human visual similarity. *Memory & Cognition*, 53(1):219–241, 2025.
- Kushin Mukherjee, Holly Huey, Martin N Hebart, and Wilma A Bainbridge 10. Drawings of things: A large-scale drawing dataset of 1,854 object concepts. *PsyArXiv*.
- Kushin Mukherjee, Karen Schloss, Laurent Lessard, Michael Gleicher, and Timothy Rogers. Color-concept associations reveal an abstract conceptual space. *Journal of Vision*, 22(14):4408–4408, 2022.
- Kushin Mukherjee, Holly Huey, Xuanchen Lu, Yael Vinker, Rio Aguina-Kang, Ariel Shamir, and Judith Fan. Seva: Leveraging sketches to evaluate alignment between human and machine visual abstraction. *Advances in Neural Information Processing Systems*, 36:67138–67155, 2023a.
- Kushin Mukherjee, Siddharth Suresh, and Timothy T. Rogers. Human-machine cooperation for semantic feature listing, 2023b. URL https://arxiv.org/abs/2304.05012. ICLR 2023 Tiny Papers.
- Kushin Mukherjee, Timothy T. Rogers, and Karen B. Schloss. Large language models estimate fine-grained human color-concept associations, 2024. URL https://arxiv.org/abs/2406.17781.
- Kushin Mukherjee, Donghao Ren, Dominik Moritz, and Yannick Assogba. Encqa: Benchmarking vision-language models on visual encodings for charts. *arXiv* preprint arXiv:2508.04650, 2025.
- S. Mukherjee, A. Mitra, G. Jawahar, et al. Orca: Progressive learning from complex explanation traces of gpt-4. arXiv:2306.02707, June 2023c.
- Marieke Mur, Mirjam Meys, Jerzy Bodurka, Rainer Goebel, Peter A Bandettini, and Nikolaus Kriegeskorte. Human object-similarity judgments reflect and transcend the primate-it object representation. *Frontiers in psychology*, 4:128, 2013.
- Lukas Muttenthaler, Jonas Dippel, Lorenz Linhardt, Robert A Vandermeulen, and Simon Kornblith. Human alignment of neural network representations. *arXiv preprint arXiv:2211.01201*, 2022a.
- Lukas Muttenthaler, Charles Y Zheng, Patrick McClure, Robert A Vandermeulen, Martin N Hebart, and Francisco Pereira. Vice: Variational interpretable concept embeddings. Advances in Neural Information Processing Systems, 35:33661–33675, 2022b.
- Lukas Muttenthaler, Klaus Greff, Frieda Born, Bernhard Spitzer, Simon Kornblith, Michael C Mozer, Klaus-Robert MÞller, Thomas Unterthiner, and Andrew K Lampinen. Aligning machine and human visual representations across abstraction levels. *arXiv preprint arXiv:2409.06509*, 2024.
- Joosung Nam, Juyeon Lee, Dongkeun Chung, Juyoung Song, Sangwoo Yoon, Sungjin Jung, Seungjong Min, and Yongjin Choi. Idealignbench: Measuring and improving value alignment of large language models. *arXiv preprint arXiv:2412.03924*, 2024.

- Hamed Nili, Cai Wingfield, Alexander Walther, Li Su, William Marslen-Wilson, and Nikolaus Kriegeskorte. A toolbox for representational similarity analysis. *PLoS computational biology*, 10(4):e1003553, 2014.
- Antonio Norelli, Marco Fumero, Valentino Maiorca, Luca Moschella, Emanuele Rodolà, and Francesco Locatello. Asif: coupled data turns unimodal models to multimodal without training. arXiv preprint arXiv:2210.01738, 2023.
- Robert M Nosofsky. Choice, similarity, and the context theory of classification. *Journal of Experimental Psychology: Learning, memory, and cognition*, 10(1):104, 1984.
- Urvashi Oswal, Christopher Cox, Matthew Lambon-Ralph, Timothy Rogers, and Robert Nowak. Representational similarity learning with application to brain networks. In *International Conference on Machine Learning*, pp. 1041–1049. PMLR, 2016.
- Long Ouyang, Jeffrey Wu, Xu Jiang, Diogo Almeida, Carroll Wainwright, Pamela Mishkin, Chong Zhang, Sandhini Agarwal, Katarina Slama, Alex Ray, et al. Training language models to follow instructions with human feedback. Advances in Neural Information Processing Systems, 35: 27730–27744, 2022.
- Karalyn Patterson, Peter J Nestor, and Timothy T Rogers. Where do you know what you know? the representation of semantic knowledge in the human brain. *Nature reviews neuroscience*, 8(12): 976–987, 2007.
- Joshua C Peterson, Joshua T Abbott, and Thomas L Griffiths. Evaluating (and improving) the correspondence between deep neural networks and human representations. *Cognitive science*, 42 (8):2648–2669, 2018.
- Hieu Pham, Zihang Dai, Golnaz Ghiasi, Hanxiao Liu, Adams Wei Yu, Minh-Thang Luong, Mingxing Tan, and Quoc V Le. Combined scaling for zero-shot transfer learning. *Neurocomputing*, 555:126658, 2022.
- Yulu Qin, Dheeraj Varghese, Adam Dahlgren Lindström, Lucia Donatelli, Kanishka Misra, and Najoung Kim. Vision-and-language training helps deploy taxonomic knowledge but does not fundamentally alter it. *arXiv preprint arXiv:2507.13328*, 2025.
- Qwen Team. Qwen technical report (tongyi qianwen). Alibaba Cloud, August 2023. [Online]. Available: https://github.com/QwenLM.
- Alec Radford, Jong Wook Kim, Chris Hallacy, Aditya Ramesh, Gabriel Goh, Sandhini Agarwal, Girish Sastry, Amanda Askell, Pamela Mishkin, Jack Clark, et al. Learning transferable visual models from natural language supervision. *International conference on machine learning*, pp. 8748–8763, 2021.
- Rafael Rafailov, Archit Sharma, Eric Mitchell, Stefano Ermon, Christopher D Manning, and Chelsea Finn. Direct preference optimization: Your language model is secretly a reward model. In Advances in Neural Information Processing Systems, volume 36, pp. 33499–33530, 2023.
- C. Raffel, N. Shazeer, A. Roberts, et al. Exploring the limits of transfer learning with a unified text-to-text transformer. *Journal of Machine Learning Research*, 21(140), 2020.
- Vedant Rathi, Abhishek Kumar, et al. Can language models learn to skip steps? arXiv preprint arXiv:2411.01855, 2024.
- David Rein, Adarsh Raichur, Andre Csiszar, Ruben Gonzalez, Bomee Yuan, Vincent Zhong, Yi Tay, Surbhi Narang, and Dani Yogatama. GPQA: A graduate-level google-proof q&a benchmark. *arXiv preprint arXiv:2311.12022*, 2023.
- David Rein, Betty Li Hou, Asa Cooper Stickland, Jackson Petty, Richard Yuanzhe Pang, Julien Dirani, Julian Michael, and Samuel R Bowman. Gpqa: A graduate-level google-proof q&a benchmark. In *First Conference on Language Modeling*, 2024.
- Timothy T Rogers and James L McClelland. Semantic cognition: A parallel distributed processing approach. MIT press, 2004.

Eleanor Rosch. Cognitive representations of semantic categories. *Journal of experimental psychology: General*, 104(3):192, 1975.

David E Rumelhart, James L McClelland, PDP Research Group, et al. *Parallel distributed processing, volume 1: Explorations in the microstructure of cognition: Foundations.* The MIT press, 1986.

Andrew M Saxe, James L McClelland, and Surya Ganguli. A mathematical theory of semantic development in deep neural networks. *Proceedings of the National Academy of Sciences*, 116 (23):11537–11546, 2019.

Peter H Schönemann. A generalized solution of the orthogonal procrustes problem. *Psychometrika*, 31(1):1–10, 1966.

Noam Shazeer. Glu variants improve transformer. arXiv preprint arXiv:2002.05202, 2020.

Roger N Shepard. Multidimensional scaling, tree-fitting, and clustering. *Science*, 210(4468):390–398, 1980.

Scott Sievert, Robert Nowak, and Timothy T Rogers. Efficiently learning relative similarity embeddings with crowdsourcing. *Journal of open source software*, 8(84), 2023.

Aarohi Srivastava, Abhinav Rastogi, Abhishek Rao, Abu Awal Md Shoeb, Abubakar Abid, Adam Fisch, Adam R. Brown, Adam Santoro, Aditya Gupta, Adrià Garriga-Alonso, Agnieszka Kluska, Aitor Lewkowycz, Akshat Agarwal, Alethea Power, Alex Ray, Alex Warstadt, Alexander W. Kocurek, Ali Safaya, Ali Tazarv, Alice Xiang, Alicia Parrish, Allen Nie, Aman Hussain, Amanda Askell, Amanda Dsouza, Ambrose Slone, Ameet Rahane, Anantharaman S. Iyer, Anders Andreassen, Andrea Madotto, Andrea Santilli, Andreas Stuhlmüller, Andrew Dai, Andrew La, Andrew Lampinen, Andy Zou, Angela Jiang, Angelica Chen, Anh Vuong, Animesh Gupta, Anna Gottardi, Antonio Norelli, Anu Venkatesh, Arash Gholamidavoodi, Arfa Tabassum, Arul Menezes, Arun Kirubarajan, Asher Mullokandov, Ashish Sabharwal, Austin Herrick, Avia Efrat, Aykut Erdem, Ayla Karakas, B. Ryan Roberts, Bao Sheng Loe, Barret Zoph, Bartłomiej Bojanowski, Batuhan Özyurt, Behnam Hedayatnia, Behnam Neyshabur, Benjamin Inden, Benno Stein, Berk Ekmekci, Bill Yuchen Lin, Blake Howald, Bryan Orinion, Cameron Diao, Cameron Dour, Catherine Stinson, Cedrick Argueta, César Ferri Ramírez, Chandan Singh, Charles Rathkopf, Chenlin Meng, Chitta Baral, Chiyu Wu, Chris Callison-Burch, Chris Waites, Christian Voigt, Christopher D. Manning, Christopher Potts, Cindy Ramirez, Clara E. Rivera, Clemencia Siro, Colin Raffel, Courtney Ashcraft, Cristina Garbacea, Damien Sileo, Dan Garrette, Dan Hendrycks, Dan Kilman, Dan Roth, Daniel Freeman, Daniel Khashabi, Daniel Levy, Daniel Moseguí González, Danielle Perszyk, Danny Hernandez, Dangi Chen, Daphne Ippolito, Dar Gilboa, David Dohan, David Drakard, David Jurgens, Debajyoti Datta, Deep Ganguli, Denis Emelin, Denis Kleyko, Deniz Yuret, Derek Chen, Derek Tam, Dieuwke Hupkes, Diganta Misra, Dilyar Buzan, Dimitri Coelho Mollo, Diyi Yang, Dong-Ho Lee, Dylan Schrader, Ekaterina Shutova, Ekin Dogus Cubuk, Elad Segal, Eleanor Hagerman, Elizabeth Barnes, Elizabeth Donoway, Ellie Paylick, Emanuele Rodola, Emma Lam, Eric Chu, Eric Tang, Erkut Erdem, Ernie Chang, Ethan A. Chi, Ethan Dyer, Ethan Jerzak, Ethan Kim, Eunice Engefu Manyasi, Evgenii Zheltonozhskii, Fanyue Xia, Fatemeh Siar, Fernando Martínez-Plumed, Francesca Happé, Francois Chollet, Frieda Rong, Gaurav Mishra, Genta Indra Winata, Gerard de Melo, Germán Kruszewski, Giambattista Parascandolo, Giorgio Mariani, Gloria Wang, Gonzalo Jaimovitch-López, Gregor Betz, Guy Gur-Ari, Hana Galijasevic, Hannah Kim, Hannah Rashkin, Hannaneh Hajishirzi, Harsh Mehta, Hayden Bogar, Henry Shevlin, Hinrich Schütze, Hiromu Yakura, Hongming Zhang, Hugh Mee Wong, Ian Ng, Isaac Noble, Jaap Jumelet, Jack Geissinger, Jackson Kernion, Jacob Hilton, Jaehoon Lee, Jaime Fernández Fisac, James B. Simon, James Koppel, James Zheng, James Zou, Jan Kocoń, Jana Thompson, Janelle Wingfield, Jared Kaplan, Jarema Radom, Jascha Sohl-Dickstein, Jason Phang, Jason Wei, Jason Yosinski, Jekaterina Novikova, Jelle Bosscher, Jennifer Marsh, Jeremy Kim, Jeroen Taal, Jesse Engel, Jesujoba Alabi, Jiacheng Xu, Jiaming Song, Jillian Tang, Joan Waweru, John Burden, John Miller, John U. Balis, Jonathan Batchelder, Jonathan Berant, Jörg Frohberg, Jos Rozen, Jose Hernandez-Orallo, Joseph Boudeman, Joseph Guerr, Joseph Jones, Joshua B. Tenenbaum, Joshua S. Rule, Joyce Chua, Kamil Kanclerz, Karen Livescu, Karl Krauth, Karthik Gopalakrishnan, Katerina Ignatyeva, Katja Markert, Kaustubh D. Dhole, Kevin Gimpel, Kevin Omondi, Kory Mathewson, Kristen Chiafullo,

Ksenia Shkaruta, Kumar Shridhar, Kyle McDonell, Kyle Richardson, Laria Reynolds, Leo Gao, Li Zhang, Liam Dugan, Lianhui Qin, Lidia Contreras-Ochando, Louis-Philippe Morency, Luca Moschella, Lucas Lam, Lucy Noble, Ludwig Schmidt, Luheng He, Luis Oliveros Colón, Luke Metz, Lütfi Kerem Şenel, Maarten Bosma, Maarten Sap, Maartje ter Hoeve, Maheen Farooqi, Manaal Faruqui, Mantas Mazeika, Marco Baturan, Marco Marelli, Marco Maru, Maria Jose Ramírez Quintana, Marie Tolkiehn, Mario Giulianelli, Martha Lewis, Martin Potthast, Matthew L. Leavitt, Matthias Hagen, Mátyás Schubert, Medina Orduna Baitemirova, Melody Arnaud, Melvin McElrath, Michael A. Yee, Michael Cohen, Michael Gu, Michael Ivanitskiy, Michael Starritt, Michael Strube, Michael Swedrowski, Michele Bevilacqua, Michihiro Yasunaga, Mihir Kale, Mike Cain, Mimee Xu, Mirac Suzgun, Mitch Walker, Mo Tiwari, Mohit Bansal, Moin Aminnaseri, Mor Geva, Mozhdeh Gheini, Mukund Varma T, Nanyun Peng, Nathan A. Chi, Nayeon Lee, Neta Gur-Ari Krakover, Nicholas Cameron, Nicholas Roberts, Nick Doiron, Nicole Martinez, Nikita Nangia, Niklas Deckers, Niklas Muennighoff, Nitish Shirish Keskar, Niveditha S. Iyer, Noah Constant, Noah Fiedel, Nuan Wen, Oliver Zhang, Omar Agha, Omar Elbaghdadi, Omer Levy, Owain Evans, Pablo Antonio Moreno Casares, Parth Doshi, Pascale Fung, Paul Pu Liang, Paul Vicol, Pegah Alipoormolabashi, Peiyuan Liao, Percy Liang, Peter Chang, Peter Eckersley, Phu Mon Htut, Pinyu Hwang, Piotr Miłkowski, Piyush Patil, Pouya Pezeshkpour, Priti Oli, Qiaozhu Mei, Qing Lyu, Qinlang Chen, Rabin Banjade, Rachel Etta Rudolph, Raefer Gabriel, Rahel Habacker, Ramon Risco, Raphaël Millière, Rhythm Garg, Richard Barnes, Rif A. Saurous, Riku Arakawa, Robbe Raymaekers, Robert Frank, Rohan Sikand, Roman Novak, Roman Sitelew, Ronan LeBras, Rosanne Liu, Rowan Jacobs, Rui Zhang, Ruslan Salakhutdinov, Ryan Chi, Ryan Lee, Ryan Stovall, Ryan Teehan, Rylan Yang, Sahib Singh, Saif M. Mohammad, Sajant Anand, Sam Dillavou, Sam Shleifer, Sam Wiseman, Samuel Gruetter, Samuel R. Bowman, Samuel S. Schoenholz, Sanghyun Han, Sanjeev Kwatra, Sarah A. Rous, Sarik Ghazarian, Sayan Ghosh, Sean Casey, Sebastian Bischoff, Sebastian Gehrmann, Sebastian Schuster, Sepideh Sadeghi, Shadi Hamdan, Sharon Zhou, Shashank Srivastava, Sherry Shi, Shikhar Singh, Shima Asaadi, Shixiang Shane Gu, Shubh Pachchigar, Shubham Toshniwal, Shyam Upadhyay, Shyamolima, Debnath, Siamak Shakeri, Simon Thormeyer, Simone Melzi, Siva Reddy, Sneha Priscilla Makini, Soo-Hwan Lee, Spencer Torene, Sriharsha Hatwar, Stanislas Dehaene, Stefan Divic, Stefano Ermon, Stella Biderman, Stephanie Lin, Stephen Prasad, Steven T. Piantadosi, Stuart M. Shieber, Summer Misherghi, Svetlana Kiritchenko, Swaroop Mishra, Tal Linzen, Tal Schuster, Tao Li, Tao Yu, Tariq Ali, Tatsu Hashimoto, Te-Lin Wu, Théo Desbordes, Theodore Rothschild, Thomas Phan, Tianle Wang, Tiberius Nkinyili, Timo Schick, Timofei Kornev, Titus Tunduny, Tobias Gerstenberg, Trenton Chang, Trishala Neeraj, Tushar Khot, Tyler Shultz, Uri Shaham, Vedant Misra, Vera Demberg, Victoria Nyamai, Vikas Raunak, Vinay Ramasesh, Vinay Uday Prabhu, Vishakh Padmakumar, Vivek Srikumar, William Fedus, William Saunders, William Zhang, Wout Vossen, Xiang Ren, Xiaoyu Tong, Xinran Zhao, Xinyi Wu, Xudong Shen, Yadollah Yaghoobzadeh, Yair Lakretz, Yangqiu Song, Yasaman Bahri, Yejin Choi, Yichi Yang, Yiding Hao, Yifu Chen, Yonatan Belinkov, Yu Hou, Yufang Hou, Yuntao Bai, Zachary Seid, Zhuoye Zhao, Zijian Wang, Zijie J. Wang, Zirui Wang, and Ziyi Wu. Beyond the imitation game: Quantifying and extrapolating the capabilities of language models, 2023. URL https://arxiv.org/abs/2206.04615.

Zach Studdiford, Timothy T Rogers, Siddharth Suresh, and Kushin Mukherjee. Evaluating steering techniques using human similarity judgments. *arXiv preprint arXiv:2505.19333*, 2025.

Ilia Sucholutsky and Thomas L. Griffiths. Alignment with human representations supports robust few-shot learning, 2023a. URL https://arxiv.org/abs/2301.11990.

Ilia Sucholutsky and Tom Griffiths. Alignment with human representations supports robust few-shot learning. *Advances in Neural Information Processing Systems*, 36:73464–73479, 2023b.

Ilia Sucholutsky, Lukas Muttenthaler, Adrian Weller, Andi Peng, Andreea Bobu, Been Kim, Bradley C Love, Erin J Achterberg, Christiane Fellbaum, Marek Grzes, et al. Getting aligned on representational alignment. *arXiv preprint arXiv:2310.13018*, 2023.

Siddharth Suresh, Kushin Mukherjee, and Timothy T. Rogers. Semantic feature verification in FLAN-T5, 2023a. URL https://arxiv.org/abs/2304.05591. ICLR 2023 Tiny Papers.

- Siddharth Suresh, Kushin Mukherjee, Xizheng Yu, Wei-Chun Huang, Lisa Padua, and Timothy Rogers. Conceptual structure coheres in human cognition but not in large language models. In Houda Bouamor, Juan Pino, and Kalika Bali (eds.), *Proceedings of the 2023 Conference on Empirical Methods in Natural Language Processing*, pp. 722–738, Singapore, December 2023b. Association for Computational Linguistics. doi: 10.18653/v1/2023.emnlp-main.47. URL https://aclanthology.org/2023.emnlp-main.47/.
- Siddharth Suresh, Wei-Chun Huang, Kushin Mukherjee, and Timothy T. Rogers. Categories vs semantic features: What shape the similarities people discern in photographs of objects? In *ICLR* 2024 Workshop on Representational Alignment, 2024. URL https://openreview.net/forum?id=iE5aXw3RFd.
- Siddharth Suresh, Kushin Mukherjee, Tyler Giallanza, Xizheng Yu, Mia Patil, Jonathan D. Cohen, and Timothy T. Rogers. Ai-enhanced semantic feature norms for 786 concepts, 2025. URL https://arxiv.org/abs/2505.10718. Also presented at the ICLR 2025 Workshop on Bidirectional Human-AI Alignment.
- Mirac Suzgun, Nathan Scales, Nathanael Schärli, Sebastian Gehrmann, Yi Tay, Hyung Won Chung, Aakanksha Chowdhery, Quoc V Le, Ed H Chi, Denny Zhou, et al. Challenging big-bench tasks and whether chain-of-thought can solve them. *arXiv preprint arXiv:2210.09261*, 2022.
- Omer Tamuz, Ce Liu, Serge Belongie, Ohad Shamir, and Adam Tauman Kalai. Adaptively learning the crowd kernel. In *International Conference on Machine Learning*, pp. 673–680, 2011.
- Tristan Thrush, Ryan Jiang, Max Bartolo, Amanpreet Singh, Adina Williams, Douwe Kiela, and Candace Ross. Winoground: Probing vision and language models for visio-linguistic compositionality. *Proceedings of the IEEE/CVF Conference on Computer Vision and Pattern Recognition*, pp. 5238–5248, 2022.
- Shengbang Tong, Erik Ferrara, Jie Wu, et al. Mass-producing failures of multimodal systems with language models. *arXiv preprint arXiv:2306.12105*, 2024.
- Greta Tuckute, Nancy Kanwisher, and Evelina Fedorenko. Language in brains, minds, and machines. *Annual Review of Neuroscience*, 47(2024):277–301, 2024.
- Amos Tversky. Features of similarity. *Psychological review*, 84(4):327, 1977.
- Aaron R Voelker and Chris Eliasmith. Improving spiking dynamical networks: Accurate delays, higher-order synapses, and time cells. *Neural computation*, 30(3):569–609, 2018.
- Catherine Wah, Steve Branson, Pietro Perona, and Serge Belongie. Similarity comparisons for interactive fine-grained categorization. *Proceedings of the IEEE Conference on Computer Vision and Pattern Recognition*, pp. 859–866, 2014.
- Alex Warstadt, Aaron Mueller, Leshem Choshen, Ethan Wilcox, Chengxu Zhuang, Juan Ciro, Rafael Mosquera, Bhargavi Paranjape, Adina Williams, Tal Linzen, et al. Findings of the babylm challenge: Sample-efficient pretraining on developmentally plausible corpora. *arXiv* preprint arXiv:2504.08165, 2025.
- Jason Wei, Maarten Bosma, Vincent Y Zhao, Kelvin Guu, Ankur Pasupat, Stella Wang, Quoc Le, and Denny Zhou. Finetuned language models are zero-shot learners. *arXiv preprint arXiv:2109.01652*, 2021.
- Alex H Williams, Erin Kunz, Simon Kornblith, and Scott W Linderman. Generalized shape metrics on neural representations. Advances in Neural Information Processing Systems, 34:4738–4750, 2021.
- Catherine Wong, William P McCarthy, Gabriel Grand, Yoni Friedman, Joshua B Tenenbaum, Jacob Andreas, Robert D Hawkins, and Judith E Fan. Identifying concept libraries from language about object structure. *arXiv preprint arXiv:2205.05666*, 2022.

- Lionel Wong, Katherine M Collins, Lance Ying, Cedegao E Zhang, Adrian Weller, Tobias Gerstenberg, Timothy O'Donnell, Alexander K Lew, Jacob D Andreas, Joshua B Tenenbaum, et al. Modeling open-world cognition as on-demand synthesis of probabilistic models. *arXiv* preprint arXiv:2507.12547, 2025.
- Daniel LK Yamins and James J DiCarlo. Using goal-driven deep learning models to understand sensory cortex. *Nature neuroscience*, 19(3):356–365, 2016.
- Daniel LK Yamins, Ha Hong, Charles F Cadieu, Ethan A Solomon, Darren Seibert, and James J DiCarlo. Performance-optimized hierarchical models predict neural responses in higher visual cortex. *Proceedings of the national academy of sciences*, 111(23):8619–8624, 2014.
- Lance Ying, Katherine M Collins, Lionel Wong, Ilia Sucholutsky, Ryan Liu, Adrian Weller, Tianmin Shu, Thomas L Griffiths, and Joshua B Tenenbaum. On benchmarking human-like intelligence in machines. *arXiv preprint arXiv:2502.20502*, 2025.
- Mert Yuksekgonul, Federico Bianchi, Pratyusha Kalluri, Dan Jurafsky, and James Zou. When and why vision-language models behave like bags-of-words, and what to do about it? *International Conference on Learning Representations*, 2023.
- Jure Zbontar, Li Jing, Ishan Misra, Yann LeCun, and Stéphane Deny. Barlow twins: Self-supervised learning via redundancy reduction. *International Conference on Machine Learning*, pp. 12310– 12320, 2021.
- Xiaohua Zhai, Alexander Kolesnikov, Neil Houlsby, and Lucas Beyer. Scaling vision transformers. *Proceedings of the IEEE/CVF Conference on Computer Vision and Pattern Recognition*, pp. 12104–12113, 2022.
- Bonan Zhao, Christopher G Lucas, and Neil R Bramley. A model of conceptual bootstrapping in human cognition. *Nature Human Behaviour*, 8(1):125–136, 2024.
- Kuan Lok Zhou, Jiayi Chen, Siddharth Suresh, Reuben Narad, Timothy T Rogers, Lalit K Jain, Robert D Nowak, Bob Mankoff, and Jifan Zhang. Bridging the creativity understanding gap: Small-scale human alignment enables expert-level humor ranking in llms. arXiv preprint arXiv:2502.20356, 2025.
- Yixin Zhou, Le Zhang, Chengyu Liu, Yinsong Yao, Yansong Feng, Yunzhe Wang, Linyi Zheng, Chenghua Zhu, Jiayi Li, Binyuan Li, Libin Wang, Ruyi Chen, Jia Guo, and Lifeng Li. IFEval: A new rigorous evaluation for instruction-following models. *arXiv preprint arXiv:2403.09886*, 2024.
- Chengxu Zhuang, Siming Yan, Aran Nayebi, Martin Schrimpf, Michael C Frank, James J DiCarlo, and Daniel LK Yamins. Unsupervised neural network models of the ventral visual stream. *Proceedings of the National Academy of Sciences*, 118(3):e2014196118, 2021.

### A APPENDIX

# A.1 ODD-ONE-OUT JUDGMENTS $\rightarrow$ SPOSE ESTIMATION (HUMAN SEMANTIC EMBEDDINGS)

To establish a ground-truth human semantic space, we employ the SPoSE (Sparse Positive Similarity Embedding) framework applied to odd-one-out behavioral data from the THINGS dataset (Hebart et al., 2023).

SPoSE Algorithm. Let  $\mathcal{X} = \{1, \dots, n\}$  index n items and let  $X \in \mathbb{R}_{\geq 0}^{n \times d}$  be a nonnegative, low-dimensional embedding with rows  $x_i^{\top} \in \mathbb{R}_{\geq 0}^d$ . We define pairwise similarities using the inner product  $s_{ij} = x_i^{\top} x_j$ , yielding similarity matrix  $S = XX^{\top}$ . In an odd-one-out trial with unordered triplet  $\{i, j, k\}$ , participants select the *most similar pair* among  $\{(i, j), (i, k), (j, k)\}$ . SPoSE models this choice behavior with a multinomial logit over pairwise similarities:

$$\Pr[(i,j) \text{ chosen } | \{i,j,k\}, X] = \frac{\exp(s_{ij})}{\exp(s_{ij}) + \exp(s_{ik}) + \exp(s_{jk})}.$$
 (1)

Estimation and Implementation. The SPoSE estimate  $\hat{X}$  is obtained via a sparsity-promoting MAP program that encourages both nonnegativity and interpretability:

$$\hat{X} \in \arg\max_{X \ge 0} \Big\{ \underbrace{\sum_{t=1}^{T} \log p(y_t \mid \{i_t, j_t, k_t\}, X)}_{\text{loc-likelihood}} - \lambda \|X\|_1 \Big\}, \tag{2}$$

where  $y_t$  is the chosen pair on trial t, and  $\lambda > 0$  controls sparsity.<sup>2</sup> We use the publicly released SPoSE embeddings as our human reference space.

Dimensionality Selection. To determine the appropriate embedding dimension, we apply PCA to the released SPoSE matrix and retain the smallest d that explains at least 95% of the variance (Appendix A.7). For our corpus of n=128 concepts, this yields  $d=\hat{d}$  dimensions ([fill in]), which we use as the target dimensionality for model embeddings.

## A.2 Anchored Similarity Judgments $\rightarrow$ Ordinal Embedding (Model Semantic Embeddings)

To obtain comparable model-based semantic embeddings, we apply an ordinal embedding algorithm (Tamuz et al., 2011; Sievert et al., 2023) to model similarity judgments, creating semantic spaces where frequently co-judged similar items are positioned closer together.

Embedding Algorithm. Each triplet  $\{i,j,k\}$  from model judgments yields an ordinal constraint: "i is closer to j than to k." Let  $\{x_i^{\star}\}_{i=1}^n \subset \mathbb{R}^d$  denote the unknown true point locations we seek to estimate, with corresponding (squared) Euclidean distance matrix  $D^{\star}$ . We model the probability of observing each ordinal constraint using a standard noisy triplet model with monotone link function:

$$\Pr\left[y_{(i;i,k)} = 1\right] = f(D_{ik}^{\star} - D_{ij}^{\star}), \qquad f(0) = \frac{1}{2}. \tag{3}$$

Estimation and Implementation. The ordinal embedding algorithm minimizes crowd-kernel triplet loss (Tamuz et al., 2011) by optimizing Euclidean distances between item pairs. We minimize an empirical surrogate of the negative log-likelihood using a low-rank Gram matrix parameterization. To ensure reliable estimates, we reserve 20% of our triplet data for validation purposes and monitor crowd-kernel loss throughout the fitting procedure.

Sample Complexity Considerations. When the true embedding has rank d and triplet judgments are sampled approximately uniformly at random, finite-sample theory provides the out-of-sample prediction error bound:

$$\mathcal{E}_{\text{pred}} = \tilde{O}\left(\sqrt{\frac{d \, n \log n}{|S|}}\right), \qquad \Rightarrow \quad |S| = \tilde{\Theta}(d \, n \log n).$$
 (4)

<sup>&</sup>lt;sup>2</sup>The nonnegativity constraint and elementwise  $\ell_1$  penalty are equivalent to an exponential prior on factors and empirically yield interpretable semantic dimensions.

Thus,  $\tilde{\Theta}(nd\log n)$  triplet judgments suffice for accurate prediction of new comparisons, and at least  $\Omega(d \, n \log n)$  ordinal comparisons are information-theoretically necessary (Jain et al., 2016). Guided by this theory and setting the model embedding dimension to match the human-derived  $\hat{d}$ , we collect

$$N_{\text{triplets}} = c d n \log n$$
 (5)

triplet judgments per model, where c is chosen to balance statistical efficiency with computational constraints.

This parallel approach provides a principled framework for human-model semantic comparison. Both methods yield d-dimensional embeddings where geometric relationships reflect semantic similarities, with the SPoSE framework extracting interpretable human semantic structure and ordinal embedding converting model judgments into geometrically comparable representations with theoretically grounded sample complexity  $\tilde{\Theta}(d \, n \log n)$ .

Table 1: Model Alignment Across Training Stages

Model	Training Stage	Alignment (R <sup>2</sup> )
Instella 3B	Base Stage 1	0.106
Instella 3B	Base	0.241
Instella 3B	SFT	0.293
Instella 3B	DPO	0.374
Llama 3.1 8B	Base	0.358
Llama 3.1 8B	SFT	0.301
Llama 3.1 8B	DPO	0.352
Llama 3.1 8B	RLVR	0.424
OLMo 13B	Base	0.299
OLMo 13B	SFT	0.392
OLMo 13B	DPO	0.406
OLMo 13B	RLVR	0.414
OLMo 7B	Base	0.179
OLMo 7B	SFT	0.347
OLMo 7B	DPO	0.357
OLMo 7B	RLVR	0.241
Average	Base Stage 1	0.106
Average	Base	0.269
Average	SFT	0.333
Average	DPO	0.372
Average	RLVR	0.360

### A.3 OBJECT CONCEPTS

The following table presents the 128 concrete object concepts from the THINGS dataset used in our experiments, along with their semantic categories and definitions.

Table 2: Complete list of object concepts with categories and definitions

Concept	Category	Definition
Animal		
badger	animal	sturdy carnivorous burrowing mammal with strong claws; widely distributed in the northern hemisphere
bear	animal	massive plantigrade carnivorous or omnivorous mammals with long shaggy coats and strong claws
butterfly	animal	diurnal insect typically having a slender body with knobbed antennae and broad colorful wings

Table 2 continued from previous page

	Table 2 continued from previous page					
Concept	Category	Definition				
chipmunk	animal	a burrowing ground squirrel of western America and Asia; has cheek				
		pouches and a light and dark stripe running down the body				
cow	animal	female of domestic cattle: "'moo-cow' is a child's term"				
crow	animal	black birds having a raucous call				
fly	animal	two-winged insects characterized by active flight				
giraffe	animal	tallest living quadruped; having a spotted coat and small horns and very long neck and legs; of savannahs of tropical Africa				
grasshopper	animal	terrestrial plant-eating insect with hind legs adapted for leaping				
hyena	animal	doglike nocturnal mammal of Africa and southern Asia that feeds chiefly on carrion				
iguana	animal	large herbivorous tropical American arboreal lizards with a spiny crest along the back; used as human food in Central America and South America				
lion	animal	large gregarious predatory feline of Africa and India having a tawny coat with a shaggy mane in the male				
mosquito	animal	two-winged insect whose female has a long proboscis to pierce the skin and suck the blood of humans and animals				
mouse	animal	a hand-operated electronic device that controls the coordinates of a cursor on your computer screen as you move it around on a pad; on the bottom of the device is a ball that rolls on the surface of the pad				
owl	animal	nocturnal bird of prey with hawk-like beak and claws and large head with front-facing eyes				
parrot	animal	usually brightly colored zygodactyl tropical birds with short hooked beaks and the ability to mimic sounds				
puffin	animal	any of two genera of northern seabirds having short necks and brightly colored compressed bills				
snail	animal	freshwater or marine or terrestrial gastropod mollusk usually having an external enclosing spiral shell				
snake	animal	limbless scaly elongate reptile; some are venomous				
tarantula	animal	large hairy tropical spider with fangs that can inflict painful but not highly venomous bites				
Clothing						
bathrobe	clothing	a loose-fitting robe of towelling; worn after a bath or swim				
beanie	clothing	a small skullcap; formerly worn by schoolboys and college freshmen				
bow	clothing	a knot with two loops and loose ends; used to tie shoelaces				
bracelet	clothing	jewelry worn around the wrist for decoration				
button	clothing	a round fastener sewn to shirts and coats etc to fit through				
0.00001	• · · · · · · · · · · · · · · · · · · ·	buttonholes				
chaps	clothing	(usually in the plural) leather leggings without a seat; joined by a belt; often have flared outer flaps; worn over trousers by cowboys to				
hat	clothing	protect their legs headdress that protects the head from bad weather; has shaped				
jeans	clothing	crown and usually a brim (usually plural) close-fitting trousers of heavy denim for manual work or casual wear				
kilt	clothing	a knee-length pleated tartan skirt worn by men as part of the traditional dress in the Highlands of northern Scotland				
kimono	clothing	a loose robe; imitated from robes originally worn by Japanese				
kneepad	clothing	protective garment consisting of a pad worn by football or baseball				
-	-	or hockey players				
tuxedo uniform	clothing clothing	semiformal evening dress for men clothing of distinctive design worn by members of a particular group				
	_	as a means of identification				
veil visor	clothing	a garment that covers the head and face a brim that projects to the front to shade the eyes				
V15U1	clothing	a ornii mat projects to the front to shade the eyes				

Table 2 continued from previous page

Concept	Category	Definition
Container		
bag	container	a flexible container with a single opening
cooker	container	a utensil for cooking
doily	container	a small round piece of linen placed under a dish or bowl
fishbowl	container	a transparent bowl in which small fish are kept
honeypot	container	South African shrub whose flowers when open are cup-shaped
		resembling artichokes
thermos	container	vacuum flask that preserves temperature of hot or cold drinks
vase	container	an open jar of glass or porcelain used as an ornament or to hold flowers
Food		
appetizer	food	food or drink to stimulate the appetite (usually served before a meal
		or as the first course)
applesauce	food	puree of stewed apples usually sweetened and spiced
baklava	food	rich Middle Eastern cake made of thin layers of flaky pastry filled with nuts and honey
beer	food	a general name for alcoholic beverages made by fermenting a cereal
		(or mixture of cereals) flavored with hops
bok choy	food	Asiatic plant grown for its cluster of edible white stalks with dark
-		green leaves
bread	food	food made from dough of flour or meal and usually raised with yeast
		or baking powder and then baked
crepe	food	small very thin pancake
cupcake	food	small cake baked in a muffin tin
dessert	food	a dish served as the last course of a meal
dough	food	a flour mixture stiff enough to knead or roll
enchilada	food	tortilla with meat filling baked in tomato sauce seasoned with chili
grapefruit	food	large yellow fruit with somewhat acid juicy pulp; usual serving consists of a half
gravy	food	a sauce made by adding stock, flour, or other ingredients to the juice
Siury	1000	and fat that drips from cooking meats
hummus	food	a thick spread made from mashed chickpeas, tahini, lemon juice and
	1000	garlic; used especially as a dip for pita; originated in the Middle East
leek	food	plant having a large slender white bulb and flat overlapping dark
		green leaves; used in cooking; believed derived from the wild
		Allium ampeloprasum
mango	food	large oval tropical fruit having smooth skin, juicy aromatic pulp, and
υ		a large hairy seed
margarita	food	a cocktail made of tequila and triple sec with lime and lemon juice
mashed potato	food	potato that has been peeled and boiled and then mashed
milkshake	food	frothy drink of milk and flavoring and sometimes fruit or ice cream
oatmeal	food	porridge made of rolled oats
parfait	food	layers of ice cream and syrup and whipped cream
pumpkin	food	usually large pulpy deep-yellow round fruit of the squash family
		maturing in late summer or early autumn
quesadilla	food	a tortilla that is filled with cheese and heated
quiche	food	a tart filled with rich unsweetened custard; often contains other
		ingredients (as cheese or ham or seafood or vegetables)
ravioli	food	small circular or square cases of dough with savory fillings
sea urchin	food	shallow-water echinoderms having soft bodies enclosed in thin
		spiny globular shells
souffle	food	light fluffy dish of egg yolks and stiffly beaten egg whites mixed
	6 :	with e.g. cheese or fish or fruit
stew	food	food prepared by stewing especially meat or fish with vegetables

Table 2 continued from previous page

Concept	Category	Definition	
tortellini	food	small ring-shaped stuffed pasta	
waffle	food	pancake batter baked in a waffle iron	
wrap	food	a sandwich in which the filling is rolled up in a soft tortilla	
Furniture			
bassinet	furniture	a basket (usually hooded) used as a baby's bed	
bathtub	furniture	a relatively large open container that you fill with water and use to wash the body	
beanbag	furniture	a small cloth bag filled with dried beans; thrown in games	
bed	furniture	a piece of furniture that provides a place to sleep	
bench	furniture	a long seat for more than one person	
coaster	furniture	a covering (plate or mat) that protects the surface of a table (i.e., from the condensation on a cold glass or bottle)	
computer screen	furniture	a screen used to display the output of a computer to the user	
cot	furniture	a small bed that folds up for storage or transport	
couch	furniture	an upholstered seat for more than one person	
crib	furniture	baby bed with high sides made of slats	
Other			
album	other	a book of blank pages with pockets or envelopes; for organizing photographs or stamp collections etc	
backscratcher	other	a long-handled scratcher for scratching your back	
banjo	other	a stringed instrument of the guitar family that has long neck and circular body	
baseball	other	a ball used in playing baseball	
baseball glove	other	the handwear used by fielders in playing baseball	
bassoon	other	a double-reed instrument; the tenor of the oboe family	
beachball	other	large and light ball; for play at the seaside	
blower	other	a device that produces a current of air	
bongo	other	a small drum; played with the hands	
cannonball	other	a solid projectile that in former times was fired from a cannon	
canvas	other	an oil painting on canvas fabric	
chainsaw	other	portable power saw; teeth linked to form an endless chain	
cymbal	other	a percussion instrument consisting of a concave brass disk; makes a loud crashing sound when hit with a drumstick or when two are struck together	
doorknob	other	a knob used to release the catch when opening a door (often called 'doorhandle' in Great Britain)	
doorknocker	other	a device (usually metal and ornamental) attached by a hinge to a door	
extinguisher	other	a manually operated device for extinguishing small fires	
fire alarm	other	a device that makes a loud sound to warn people when there is a fire	
guitar	other	a stringed instrument usually having six strings; played by strumming or plucking	
hatchet	other	a small ax with a short handle used with one hand (usually to chop wood)	
hula hoop	other	a large hoop spun around the body by gyrating the hips, for play or exercise.	
knitting needle	other	needle consisting of a slender rod with pointed ends; usually used in pairs	
knob	other	a round handle	
lawnmower	other	garden tool for mowing grass on lawns	
pinball	other	a game played on a sloping board; the object is to propel marbles against pins or into pockets	
pocket watch	other	a watch that is carried in a small watch pocket	

Table 2 continued from previous page

Concept	Category	Definition
shuffleboard	other	a game in which players use long sticks to shove wooden disks onto the scoring area marked on a smooth surface
skeleton	other	the hard structure (bones and cartilages) that provides a frame for the body of an animal
swab	other	implement consisting of a small piece of cotton that is used to apply medication or cleanse a wound or obtain a specimen of a secretion
tennis ball	other	ball about the size of a fist used in playing tennis
toilet paper	other	a soft thin absorbent paper for use in toilets
treadmill	other	an exercise device consisting of an endless belt on which a person can walk or jog without changing place
trowel	other	a small hand tool with a handle and flat metal blade; used for scooping or spreading plaster or similar materials
volleyball	other	an inflated ball used in playing volleyball
Plant		
flower	plant	a plant cultivated for its blooms or blossoms
gourd	plant	any of numerous inedible fruits with hard rinds
Vehicle		
airbag	vehicle	a safety restraint in an automobile; the bag inflates on collision and prevents the driver or passenger from being thrown forward
carriage	vehicle	a vehicle with wheels drawn by one or more horses
exhaust pipe	vehicle	a pipe through which burned gases travel from the exhaust manifold to the muffler
hot-air balloon	vehicle	balloon for travel through the air in a basket suspended below a large bag of heated air
humvee	vehicle	a high mobility, multipurpose, military vehicle with four-wheel drive
missile	vehicle	a rocket carrying a warhead of conventional or nuclear explosives; may be ballistic or directed by remote control
odometer	vehicle	a meter that shows mileage traversed
taillight	vehicle	lamp (usually red) mounted at the rear of a motor vehicle
tank	vehicle	an enclosed armored military vehicle; has a cannon and moves on caterpillar treads
taxi	vehicle	a car driven by a person whose job is to take passengers where they want to go in exchange for money

### A.4 MODEL SUITE

Table 3: List of all the models used

Model		Attention Type	Training To- kens	#Heads	Hidden Dim
Falcon3-3B-Base Team (2024)	Falcon-LLM	GQA	100B	12 (4 KV)	3072
tiiuae/falcon-7b Team (2024)	Falcon-LLM	MQA	1.5T	71	4544
tiiuae/falcon-7b-ins LLM Team (2024)	struct Falcon-	MQA		71	4544
Falcon3-10B-Base Team (2024)	Falcon-LLM	GQA	2T	12 (4 KV)	3072
tiiuae/falcon-11b Team (2024)	Falcon-LLM	GQA	5T	32 (8 KV)	4096

Continued on next page

Table 3 continued from previous page					
Model	Attention Type	Training To kens	- #Heads	Hidden Dim	
flan-t5-small Chung et al. (2022) flan-t5-large Chung et al. (2022) flan-t5-xl Chung et al. (2022) flan-t5-xxl Chung et al. (2022)	Multi-Head Multi-Head Multi-Head Multi-Head		8 16 32 128	512 1024 1024 1024	
gemma-3-270m Ji et al. (2024) gemma-3-270m-it Ji et al. (2024) gemma-2-2b Ji et al. (2024) gemma-2-2b-it Ji et al. (2024) gemma-2-9b Ji et al. (2024) gemma-2-9b-it Ji et al. (2024) gemma-2-27b Ji et al. (2024) gemma-3-4b-it Ji et al. (2024) gemma-3-4b-pt Ji et al. (2024) gemma-3-12b-it Ji et al. (2024) gemma-3-12b-jt Ji et al. (2024) gemma-3-12b-jt Ji et al. (2024)	GQA GQA MQA MQA MHA MHA MHA GQA GQA GQA GQA GQA GQA		8 (shared KV) 8 (shared KV) 8 (shared KV) 16 (16 16 16 16 12 (4 KV) 12 (4 KV) 16 (4 KV) 16 (4 KV) 16 (4 KV) 16 (4 KV)	2048 2048 2048 2048 4096 4096 6144 6144 3072 3072 4096 4096 5120 5120	
GPT-OSS-20B Black et al. (2022) amd/Instella-3B Liu et al. (2025) amd/Instella-3B-Instruct Liu et al. (2025)	Multi-Head Multi-Head Multi-Head	∼300B 4.15T	64 32 32	6144 2560 2560	
Llama-3.1-8B-Instruct Meta AI (2024) state-spaces/mamba-1.4b-hf Dao	MHA (SSM)		32	4096	
et al. (2023) <b>allenai/OLMo-2-1124-7B</b> Groen- eveld et al. (2024)	MHA		32	4096	
allenai/OLMo-2-1124-7B- Instruct Groeneveld et al. (2024)	MHA		32	4096	
allenai/OLMo-2-1124-13B- Instruct Groeneveld et al. (2024) OLMo-2-1124-7B-	MHA MHA		40 32	5120 4096	
<b>DPO</b> Groeneveld et al. (2024) <b>OLMo-2-1124-7B-</b>	MHA		32	4096	
SFT Groeneveld et al. (2024) AMD-OLMo-1B Groeneveld	MHA		16	2048	
et al. (2024)  AMD-OLMo-1B-SFT-  DPO Groeneveld et al. (2024)	MHA		16	2048	
GPT-J-6B EleutherAI (2021) orca-2-7b Mukherjee et al.	Multi-Head Multi-Head	∼300B	16 32	4096 4096	
(2023c) orca-2-13b Mukherjee et al.	Multi-Head		40	5120	
(2023c) <b>phi-3.5-mini-instruct</b> Gunasekar et al. (2023)	Multi-Head		32	2048	
phi-3-mini-128k- instruct Gunasekar et al. (2023)	Multi-Head		32	2048	
<b>phi-3-medium-128k-instruct</b> Gunasekar et al. (2023)	Multi-Head		40	5120	
Phi-3-medium-4k- instruct Gunasekar et al. (2023)	Multi-Head		40	5120	

Continued on next page

Table 3 continued from previous page

Model	Attention Type	Training To- kens	#Heads	Hidden Dim
<b>phi-1_5</b> Gunasekar et al. (2023)	Multi-Head	7B	32	2048
qwen-14b Qwen Team (2023) qwen-14b-chat Qwen Team (2023)	GQA GQA	3T	40 (10 KV) 40 (10 KV)	5120 5120
qwen-2-7b Qwen Team (2023) qwen-2-7b-instruct Qwen Team (2023)	GQA GQA		32 (8 KV) 32 (8 KV)	4096 4096
<b>qwen-2.5-7b</b> Qwen Team (2023) <b>qwen-2.5-7b-instruct</b> Qwen Team (2023)	GQA GQA		32 (8 KV) 32 (8 KV)	4096 4096
<b>qwen-2.5-14b</b> Qwen Team (2023) <b>qwen-2.5-14b-instruct</b> Qwen Team (2023)	GQA GQA		40 (10 KV) 40 (10 KV)	5120 5120
<b>t5-3b</b> Raffel et al. (2020) <b>t5-11b</b> Raffel et al. (2020)	Multi-Head Multi-Head	$\sim 1T$ $\sim 1T$	32 128	1024 1024
<b>yi-9B</b> 01.AI Team (2024) <b>yi-9B (coder)</b> 01.AI Team (2024)	Multi-Head Multi-Head	3.1T 0.8T	32 32	6144 6144

### A.5 DETAILS FOR SPOSE (ODD-ONE-OUT) ESTIMATION

Given  $S = XX^{\top}$  with  $X \ge 0$ , the triplet likelihood is the three-way softmax in equation 1. The MAP program equation 2 is optimized by minibatch stochastic gradients;  $\lambda$  is tuned by held-out triplets. The released THINGS-data SPoSE embeddings are derived from large-scale odd-one-out judgments and approach the behavioral noise ceiling in predicting left-out triplets, despite far fewer than the  $O(n^3)$  triplets required to fully determine a dense similarity matrix (Hebart et al., 2023).

### A.6 ORDINAL EMBEDDING: RISK BOUNDS AND RECOVERY

Let  $G^*$  be the centered Gram matrix of  $\{x_i^*\}\subset\mathbb{R}^d$  and let  $\mathcal{L}(G)$  denote the expected logistic triplet loss induced by equation 3. If  $G^*$  has rank d and |S| triplets are drawn uniformly at random, then with probability  $1-\delta$ ,

$$\mathcal{L}(\hat{G}) - \mathcal{L}(G^{\star}) \leq C_1 \sqrt{\frac{d n \log n}{|S|}} + C_2 \sqrt{\frac{\log(1/\delta)}{|S|}}, \tag{6}$$

for universal constants  $C_1$ ,  $C_2$  depending on the loss Lipschitz constant (Jain et al., 2016). Moreover, writing  $C^*$  for the component of the EDM orthogonal to the linear operator's kernel, one can recover the distance structure with

$$\frac{1}{n^2} \|\hat{C} - C^\star\|_F^2 = \tilde{O}\left(\frac{d \, n \log n}{|S|}\right),\tag{7}$$

which implies equation 7 samples suffice up to logarithmic factors;  $\Omega(d \, n \log n)$  lower bounds are known (Jamieson & Nowak, 2011).

### A.7 DIMENSIONALITY SELECTION FROM HUMAN SPOSE

We compute PCA on the released SPoSE embedding matrix (items  $\times$  dimensions), retain the top d components explaining at least 95% variance, and set  $d=\hat{d}$  for model-side ordinal embeddings. In our corpus (n=128), this yields  $\hat{d}=29$ , and therefore  $N_{\rm triplets}=c\,\hat{d}\,n\log n=31,288$  triplets per model where c=4. We increase  $N_{\rm triplets}$  to **35,000** to provide a margin of error.

### A.8 MEASURE CORRELATIONS

#### **Correlations: Benchmarks and Human-Model Alignment 1.00** 0.44 0.67 0.43 **0.03** 0.50 0.68 0.64 0.67 ifeval - 1.0 1.00 0.72 0.88 0.50 0.94 0.74 0.70 0.64 bbh 8.0 0.19 0.84 0.61 0.57 0.51 math 0.67 0.72 1.00 0.89 0.88 0.89 1.00 0.37 0.88 0.56 0.51 0.46 0.43 gpqa 0.6 -0.03 0.50 0.19 0.37 0.45 0.36 0.34 0.33 musr 0.94 0.84 0.88 0.45 1.00 0.71 0.68 0.62 mmlu Procrustes R2 0.68 0.74 0.61 0.56 0.36 0.71 1.00 0.99 0.97 - 0.2 cka 0.64 0.70 0.57 0.51 0.34 0.68 0.99 1.00 0.98 - 0.0 RDM 0.67 0.64 0.51 0.46 0.33 0.62 procrustes R2 MUST

Figure 5: Correlations between measures of human-model alignment and model benchmarks, for models where benchmark scores are publicly are available. (Procrustes  $\mathbb{R}^2$ , CKA, RSM)

# A.9 RELATIONSHIPS BETWEEN COMPUTATIONAL INGREDIENT PROPERTIES AND HUMAN-MODEL ALIGNMENT

#### All Predictors vs. Procrustes R2 alignment Training tokens (T) 0.6 0.4 0.5 0.4 전 0.3 0.2 0.2 0.2 0.1 0.1 r=0.25, p=0.032 0.0 0.0 20 30 params\_billion Number of heads Number of KV heads Attention dimension 0.5 0.5 0.4 0.4 0.6 0.2 0.2 0.2 0.1 r=-0.07, p=0.532 125 250 0.5 0.5 • 0.4 0.4 0.4 0.3 7 0.2 0.2 0.2 0.1 0.1 r=0.10, p=0.364 50000 100000 150000 200000 250000 vocab\_size 25000 50000 75000 100000125000 max\_pos\_embed MLP dimension Model family Activation function 0.8 0.6 0.2 r=0.23, p=0.049 0.0 0.0 SwiGLU GeLU 0.5 0.4 °.0 align e 0.3 Procrustes R<sup>2</sup> a o.2 R s o.2 Stes R<sup>2</sup> 8 0.0 0.0 0.0

Figure 6: Categorical and continuous between all computational ingredients and human-model alignment. All significant effects in the full mixed linear-model are reported in the main text, Figure 2.

### A.10 t-SNE VISUALIZATIONS

Table 4: Complete ranking of models by R<sup>2</sup> score

Rank	Model Name	R <sup>2</sup> Score	Rank	Model Name	R <sup>2</sup> Score
1	qwen25-14b-instruct	0.492	39	qwen2-7b	0.294
2	Phi-3-medium-4k-instruct	0.469	40	Instella-3B-SFT	0.293
3	Phi-3.5-MoE-instruct	0.468	41	Falcon3-3B-Base	0.286
4	gemma-3-27b-it	0.460	42	flan-t5-xl	0.265
5	qwen25-7b-instruct	0.459	43	falcon-11b	0.257
6	Phi-3.5-mini-instruct	0.457	44	OLMo-2-1124-7B-Instruct	0.241
7	phi-3-medium-128k-instruct	0.450	45	Instella-3B	0.241
8	qwen2-7b-instruct	0.446	46	Falcon3-Mamba-7B-Base	0.224
9	gemma-2-9b-it	0.440	47	flan-t5-large	0.199
10	gemma-3-4b-it	0.438	48	Qwen3-4B-Base	0.194
11	gemma-2-27b-it	0.433	49	phi-1_5	0.180
12	gemma-3-12b-it	0.431	50	OLMo-2-1124-7B	0.179
13	Llama-3.1-8B-Instruct	0.424	51	gemma-2-9b	0.178
14	OLMo-2-0325-32B-Instruct	0.423	52	falcon-7b	0.175
15	qwen-14b-chat	0.418	53	OLMo-2-0425-1B-SFT	0.168
16	OLMo-2-1124-13B-Instruct	0.414	54	llama2-7b-chat	0.160
17	phi-3-mini-128k-instruct	0.412	55	gemma-3-4b-pt	0.147
18	OLMo-2-1124-13B-DPO	0.406	56	gemma-3-27b-pt	0.143
19	Falcon3-10B-Base	0.406	57	gemma-3-12b-pt	0.127
20	Phi-3.5-vision-instruct	0.400	58	gemma-2-2b	0.126
21	OLMo-2-1124-13B-SFT	0.392	59	OLMo-2-0425-1B	0.123
22	qwen3-8b	0.388	60	llama2-7b	0.122
23	Instella-3B-Instruct	0.374	61	AMD-OLMo-1B	0.113
24	gemma-2-27b	0.369	62	flan-t5-small	0.111
25	qwen25-14b	0.363	63	AMD-OLMo-1B-SFT-DPO	0.108
26	Llama-3.1-Tulu-3-8B	0.358	64	Instella-3B-Stage1	0.106
27	qwen-14b	0.357	65	qwen25-7b	0.104
28	OLMo-2-1124-7B-DPO	0.357	66	falcon-7b-instruct	0.103
29	Llama-3.1-Tulu-3-8B-DPO	0.352	67	t5-3b	0.103
30	OLMo-2-1124-7B-SFT	0.347	68	t5-11b	0.095
31	orca-2-13b	0.343	69	gemma-3-270m	0.092
32	qwen3-14b	0.337	70	Yi-9B	0.091
33	gemma-2-2b-it	0.321	71	gpt-oss-20b	0.087
34	orca-2-7b	0.315	72	gemma-3-270m-it	0.085
35	flan-t5-xxl	0.302	73	mamba-1.4b-hf	0.083
36	Llama-3.1-Tulu-3-8B-SFT	0.301	74	mamba-2.8b-hf	0.077
37	llama2-13b-chat	0.299	75	gpt-j-6b	0.025
38	OLMo-2-1124-13B	0.299			

Figure 7: t-SNE visualizations of model embeddings (Part 1). R<sup>2</sup> scores are in parentheses.

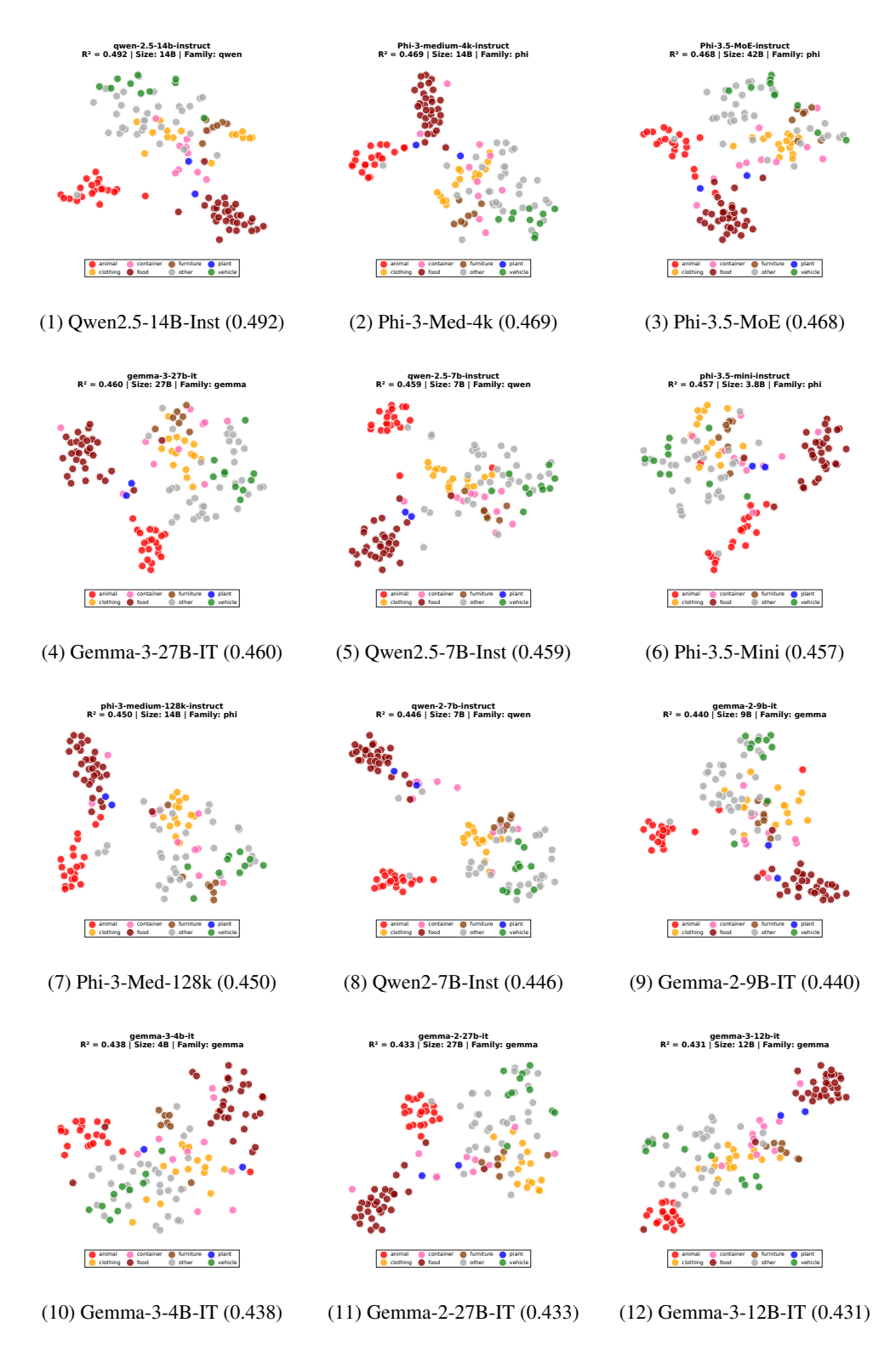


Figure 8: t-SNE visualizations of model embeddings (Part 2). R<sup>2</sup> scores are in parentheses.

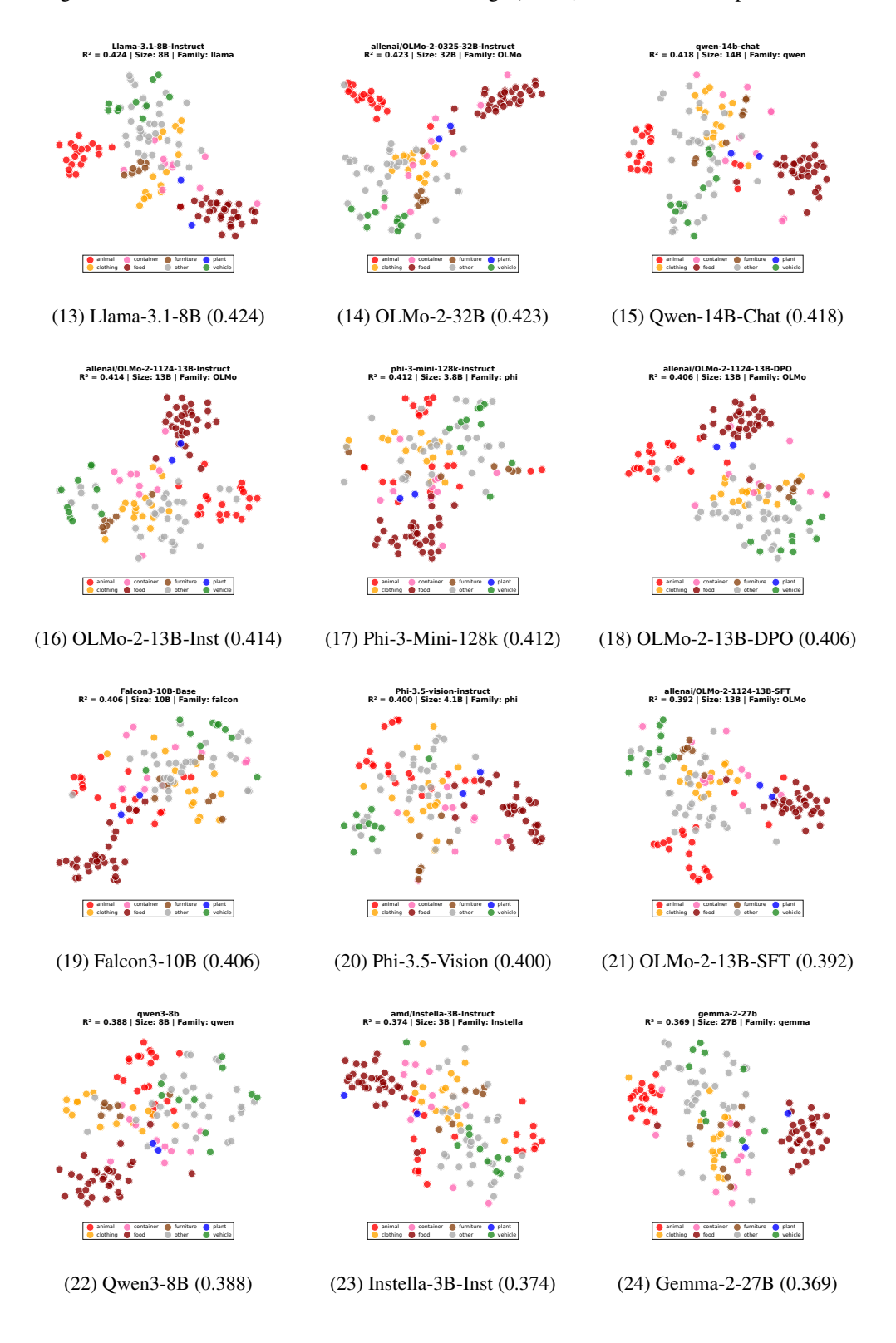


Figure 9: t-SNE visualizations of model embeddings (Part 3). R<sup>2</sup> scores are in parentheses.

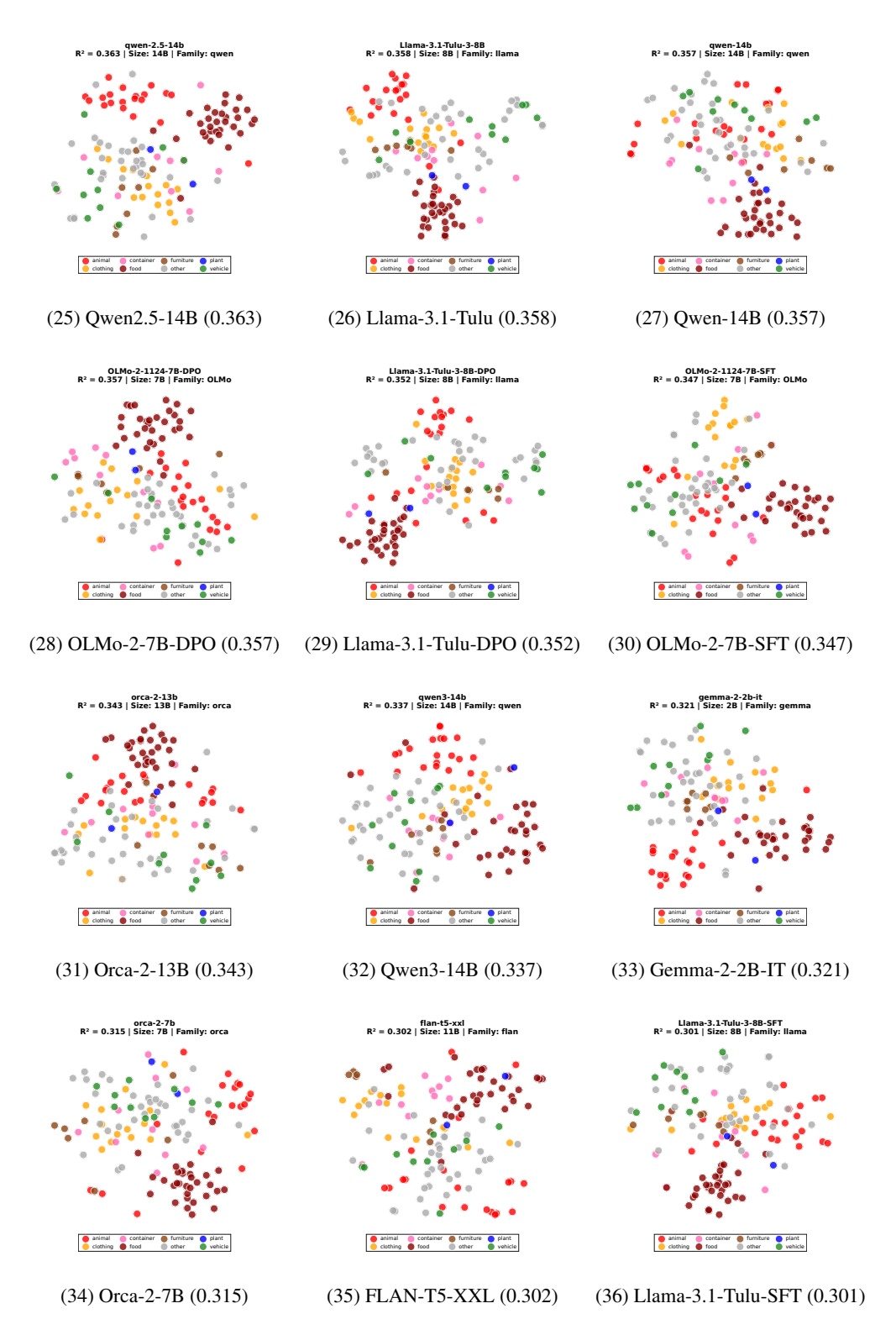


Figure 10: t-SNE visualizations of model embeddings (Part 4). R<sup>2</sup> scores are in parentheses.

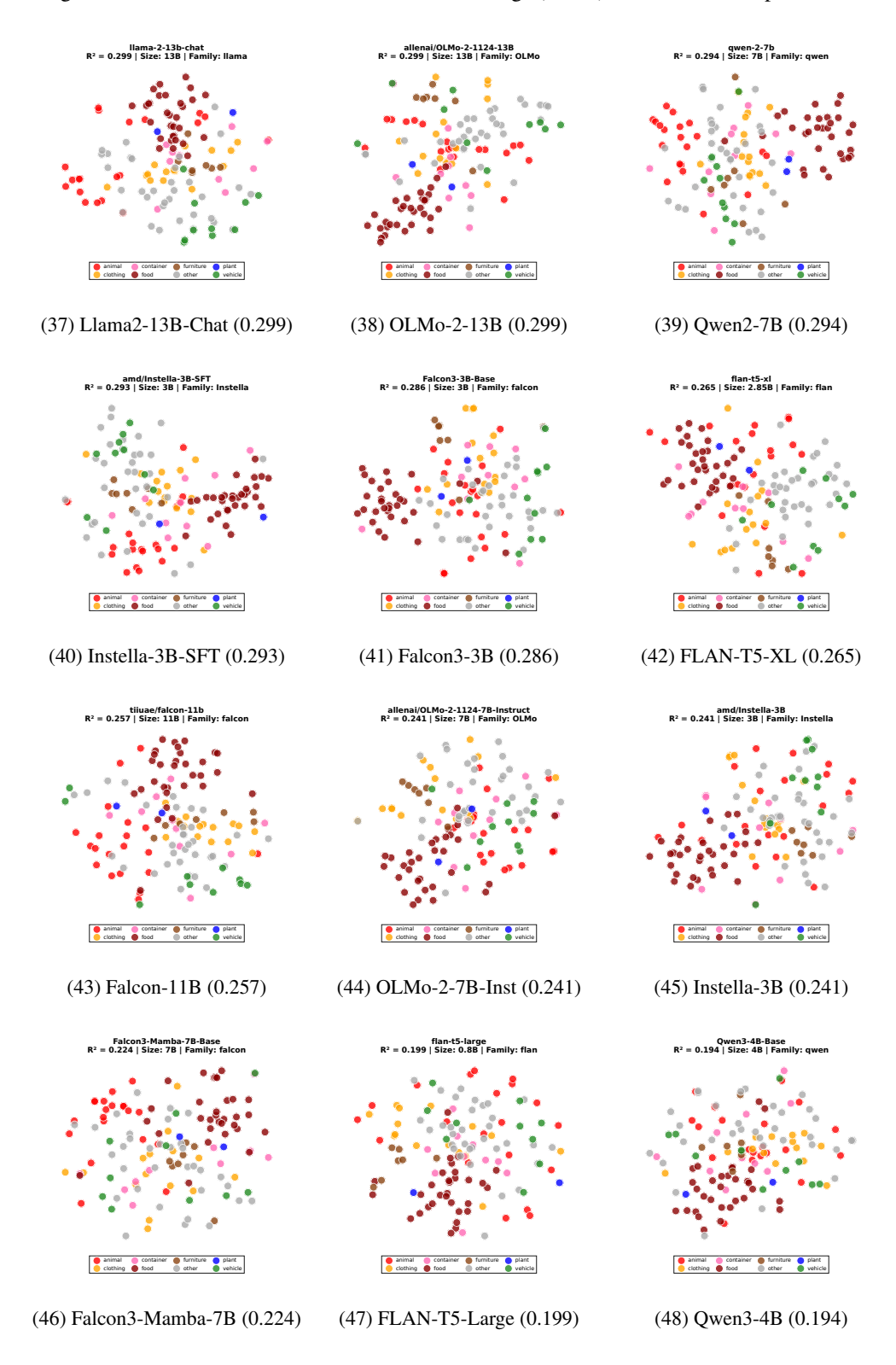


Figure 11: t-SNE visualizations of model embeddings (Part 5). R<sup>2</sup> scores are in parentheses.

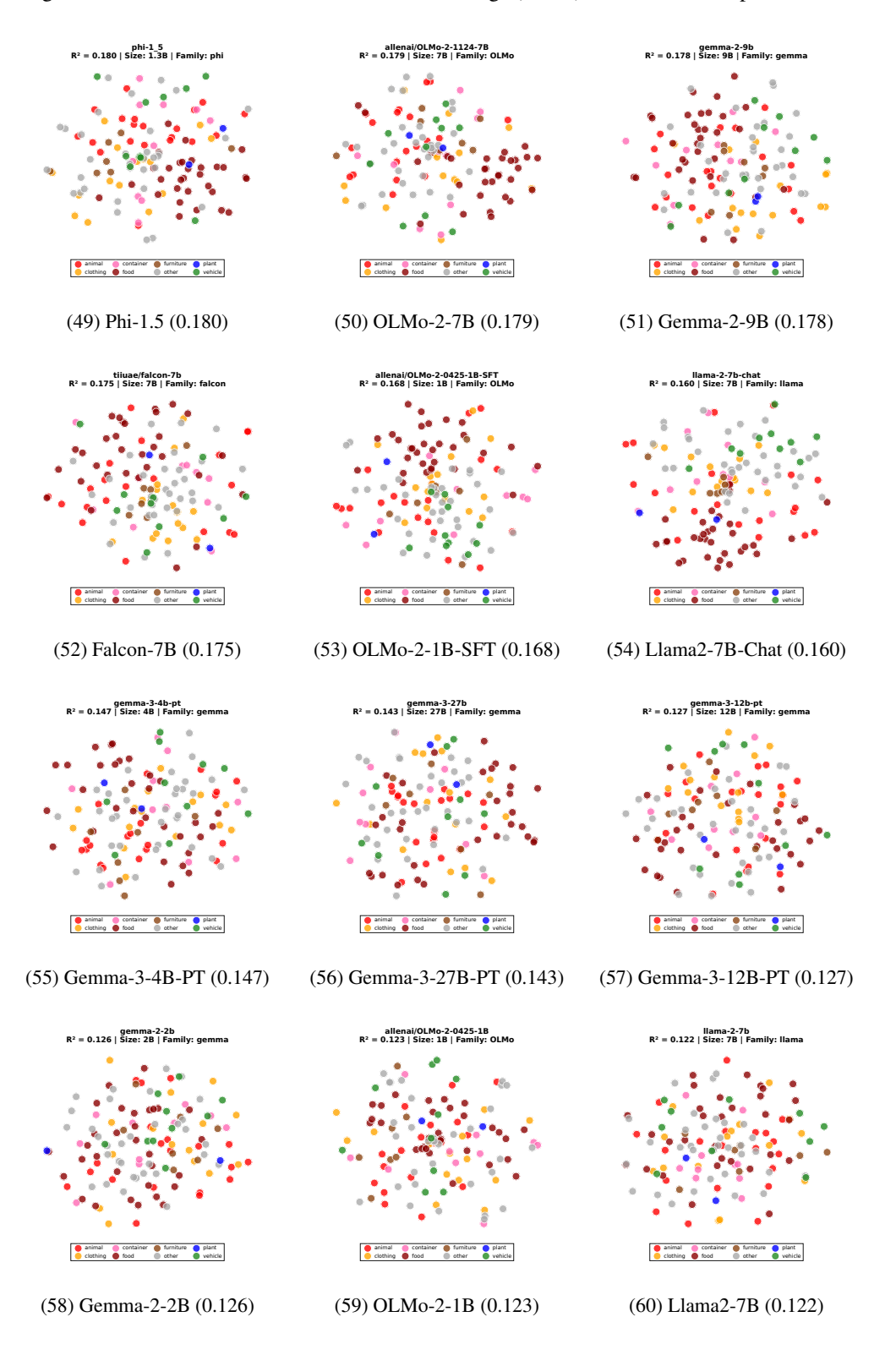


Figure 12: t-SNE visualizations of model embeddings (Part 6). R<sup>2</sup> scores are in parentheses.

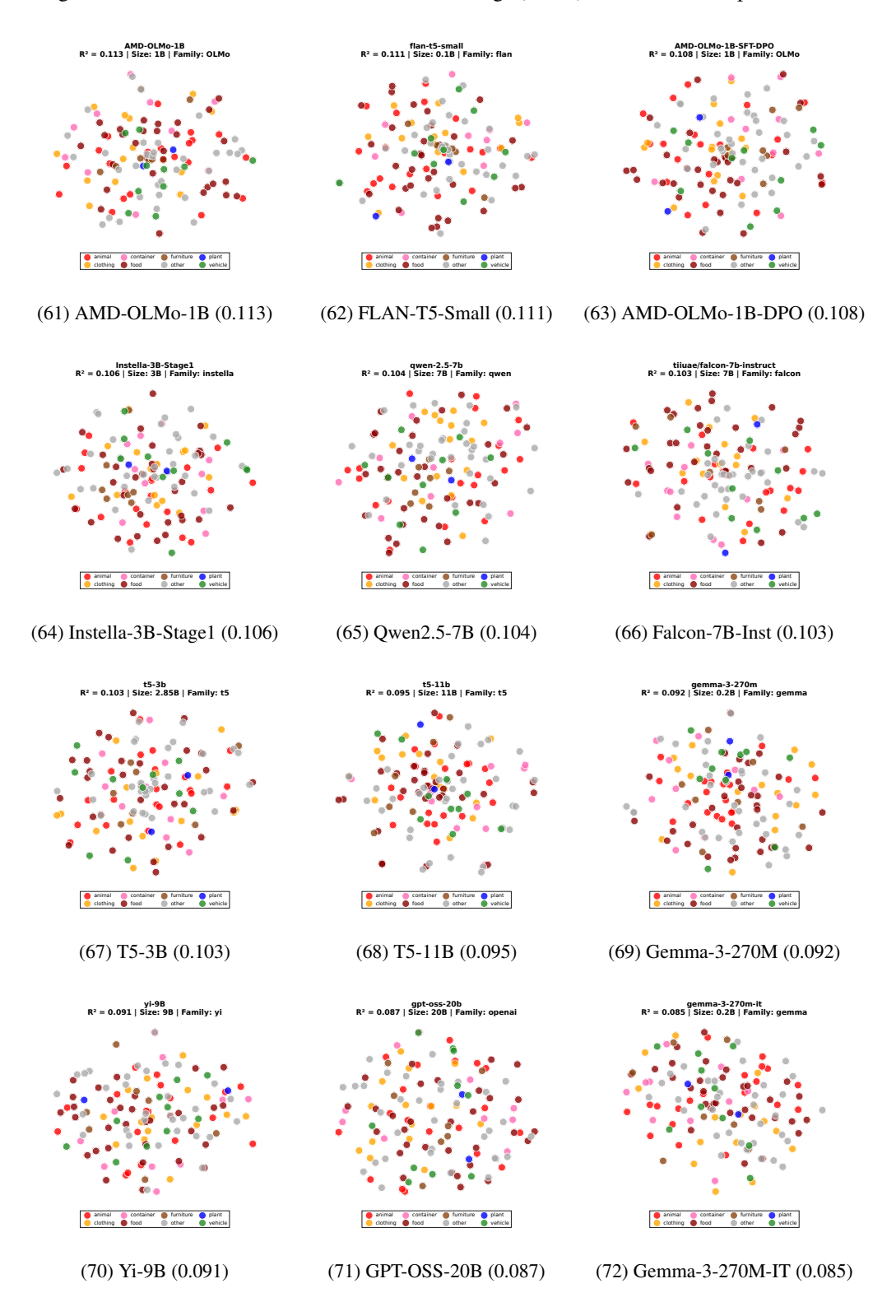


Figure 13: t-SNE visualizations of model embeddings (Part 7). R<sup>2</sup> scores are in parentheses.

